

Generation of procedural landscape

Torbjörn Rathsman

July 16, 2022

Contents

1. The height-map	9
1.1. Metrics of mountain ranges	9
1.1.1. The elevation distribution	11
1.1.2. The elevation gradient	11
1.1.3. The relation between peak and valley elevation	12
1.1.4. The average steepness as a function of direction	14
1.2. Measurements of real mountain ranges	15
1.2.1. Visual comparisons	15
1.2.2. The elevation distribution	22
1.2.3. The gradient as a function of the elevation	23
1.2.4. The relation between peak and valley elevation	23
1.2.5. The average steepness as a function of direction	34
1.3. Mathematical models to create a height-map	35
1.3.1. A simple noise-based model	35
A. Scaling factors in geodetic coordinates	40

List of Figures

1.1.	The same mountain but with different “tallness”. The low two versions classified as “low”, both have the same peak elevation, but the tall one, is considerably steeper. Also, the two versions marked as “high” shares peak elevation. The tall mountains have the same gradient, but not the same peak elevation.	13
1.2.	Height-map showing the elevation of the northern parts of the Ural mountains, retrieved from [3]. For partitioning, see table 1.2. © DLR e.V. (2014-2018) and © Airbus Defence and Space GmbH 2022 provided under COPERNICUS by the European Union and ESA; all rights reserved.	15
1.3.	Height-map showing the elevation of the southern parts of the Ural mountains, retrieved from [3]. For partitioning, see table 1.2. In order to save space, this height-map is oriented from north-south, rather than west-east. Since this part of the Ural mountains runs in the north direction and the latitude is quite high, the mountains appear stretched in the west-east direction. © DLR e.V. (2014-2018) and © Airbus Defence and Space GmbH 2022 provided under COPERNICUS by the European Union and ESA; all rights reserved.	16
1.4.	Height-map showing the elevation of the northern parts of the Scandinavian mountains, retrieved from [3]. For partitioning, see table 1.2. © DLR e.V. (2014-2018) and © Airbus Defence and Space GmbH 2022 provided under COPERNICUS by the European Union and ESA; all rights reserved.	17
1.5.	Height-map showing the elevation of the southern parts of the Scandinavian mountains, retrieved from [3]. For partitioning, see table 1.2. © DLR e.V. (2014-2018) and © Airbus Defence and Space GmbH 2022 provided under COPERNICUS by the European Union and ESA; all rights reserved.	17
1.6.	Height-map showing the elevation of the Alps, retrieved from [3]. © DLR e.V. (2014-2018) and © Airbus Defence and Space GmbH 2022 provided under COPERNICUS by the European Union and ESA; all rights reserved.	18
1.7.	Height-map showing the elevation in the Karakoram mountains, retrieved from [3]. © DLR e.V. (2014-2018) and © Airbus Defence and Space GmbH 2022 provided under COPERNICUS by the European Union and ESA; all rights reserved.	18

1.8.	A rendering from the north ridge of Masherbrum towards north-east, using a scale-corrected portion of fig. 1.7 as height-map. The aspect ratio has been set to 2.4 : 1, and the horizontal field-of-view to 54.3°	19
1.9.	A rendering from the south face of K2 towards south-west, using a scale-corrected portion of fig. 1.7 as height-map. The aspect ratio has been set to 2.4 : 1, and the horizontal field-of-view to 54.3°	20
1.10.	Height-map showing the elevation in the western parts of the Himalayas, retrieved from [3]. For partitioning, see table 1.2 © DLR e.V. (2014-2018) and © Airbus Defence and Space GmbH 2022 provided under COPERNICUS by the European Union and ESA; all rights reserved.	20
1.11.	Height-map showing the elevation in the central parts of the Himalayas, retrieved from [3]. For partitioning, see table 1.2. © DLR e.V. (2014-2018) and © Airbus Defence and Space GmbH 2022 provided under COPERNICUS by the European Union and ESA; all rights reserved.	21
1.12.	Height-map showing the elevation in the eastern parts of the Himalayas, retrieved from [3]. For partitioning, see table 1.2. © DLR e.V. (2014-2018) and © Airbus Defence and Space GmbH 2022 provided under COPERNICUS by the European Union and ESA; all rights reserved.	21
1.13.	The elevation distribution (measured in area per elevation) as a function of the elevation. Data-set numbering follows the order in table 1.2.	22
1.14.	The gradient as a function of elevation with all data-sets considered. “Model 1” uses eq. (1.3), with $z_0 = 14\,000$ m and $\alpha = 0.349$. “Model 2” uses eq. (1.5), with $A = 0.45$, $z_0 = 330$ m, $\alpha = 0.178$, and $\beta = 0.417$	24
1.15.	The gradient as a function of elevation in the northern parts of the Ural mountains. “Model 1” uses eq. (1.3), with $z_0 = 3200$ m and $\alpha = 0.874$. “Model 2” uses eq. (1.5), with $A = 1.7$, $z_0 = 2900$ m, $\alpha = 1.02$, and $\beta = 0.282$	24
1.16.	The gradient as a function of elevation in the southern parts of the Ural mountains. “Model 1” uses eq. (1.3), with $z_0 = 3200$ m, and $\alpha = 1$. “Model 2” uses eq. (1.5), with $A = 0.20$, $z_0 = 360$ m, $\alpha = 0.634$, and $\beta = 1$	25
1.17.	The gradient as a function of elevation in the northern parts of the Scandinavian mountains. “Model 1” uses eq. (1.3), with $z_0 = 1\,100\,000$ m, and $\alpha = 0.166$. “Model 2” uses eq. (1.5), with $A = 0.62$, $z_0 = 1100$ m, $\alpha = 0.236$, and $\beta = 1$	25
1.18.	The gradient as a function of elevation in the southern parts of the Scandinavian mountains. “Model 1” uses eq. (1.3), with $z_0 = 9\,900\,000$ m, and $\alpha = 0.141$. “Model 2” uses eq. (1.5), with $A = 0.21$, $z_0 = 1300$ m, $\alpha = 0.208$, and $\beta = 1$	26

1.19. The gradient as a function of elevation in the Alps. “Model 1” uses eq. (1.3), with $z_0 = 8500$ m, and $\alpha = 0.395$. “Model 2” uses eq. (1.5), with $A = 0.30$, $z_0 = 68$ m, $\alpha = 0.169$, and $\beta = 0.371$.	26
1.20. The gradient as a function of elevation in the Karakoram mountains. “Model 1” uses eq. (1.3), with $z_0 = 8000$ m, and $\alpha = 0.580$. “Model 2” uses eq. (1.5), with $A = 0.44$, $z_0 = 1300$ m, $\alpha = 9.67$, and $\beta = 0.559$.	27
1.21. The gradient as a function of elevation in the western parts of the Himalayas. “Model 1” uses eq. (1.3), with $z_0 = 9900$ m, and $\alpha = 0.432$. “Model 2” uses eq. (1.5), with $A = 0.46$, $z_0 = 460$ m, $\alpha = 2.80$, and $\beta = 0.257$.	27
1.22. The gradient as a function of elevation in the central parts of the Himalayas. “Model 1” uses eq. (1.3), with $z_0 = 12\,000$ m, and $\alpha = 0.339$. “Model 2” uses eq. (1.5), with $A = 0.43$, $z_0 = 250$ m, $\alpha = 2.94$, and $\beta = 0.230$.	28
1.23. The gradient as a function of elevation in the eastern parts of the Himalayas. “Model 1” uses eq. (1.3), with $z_0 = 19\,000$ m, and $\alpha = 0.272$. “Model 2” uses eq. (1.5), with $A = 0.625$, $z_0 = 290$ m, $\alpha = 2.06$, and $\beta = 0$.	28
1.24. Mountain tallness as a function of peak elevation with all data-sets considered. The linear model uses eq. (1.8), with $A = 8.7$. “Model 1” uses eq. (1.7), with $z_0 = 580$ m, and $\alpha = 2.75$. “Model 2” uses eq. (1.6), with $A = 720$ m, $z_0 = 5600$ m, $\alpha = 0.719$, and $\beta = 4.06$.	29
1.25. Mountain tallness as a function of peak elevation in the northern parts of the Ural mountains. The linear model uses eq. (1.8), with $A = 4.5$. “Model 1” uses eq. (1.7), with $z_0 = 7.9$ m, and $\alpha = 1.11$. “Model 2” uses eq. (1.6), with $A = 590$ m, $z_0 = 1400$ m, $\alpha = 1.27$, and $\beta = 3.21$.	29
1.26. Mountain tallness as a function of peak elevation in the southern parts of the Ural mountains. The linear model uses eq. (1.8), with $A = 4.2$. “Model 1” uses eq. (1.7), with $z_0 = 25$ m, and $\alpha = 1.48$. “Model 2” uses eq. (1.6), with $A = 590$ m, $z_0 = 1200$ m, $\alpha = 1.67$, and $\beta = 2.85$.	30
1.27. Mountain tallness as a function of peak elevation in the northern parts of the Scandinavian mountains. The linear model uses eq. (1.8), with $A = 4.9$. “Model 1” uses eq. (1.7), with $z_0 = 2.71$ m, and $\alpha = 0.904$. “Model 2” uses eq. (1.6), with parameters that makes it almost identical to Model 1.	30
1.28. Mountain tallness as a function of peak elevation in the southern parts of the Scandinavian mountains. The linear model uses eq. (1.8), with $A = 6.6$. “Model 1” uses eq. (1.7), with $z_0 = 0.93$ m, and $\alpha = 0.732$. “Model 2” uses eq. (1.6), with $A = 1000$ m, $z_0 = 5000$ m, $\alpha = 0.841$, and $\beta = 0.385$.	31

1.29. Mountain tallness as a function of peak elevation in the Alps. The linear model uses eq. (1.8), with $A = 6.5$. “Model 1” uses eq. (1.7), with $z_0 = 23$ m, and $\alpha = 1.26$. “Model 2” uses eq. (1.6), with $A = 890$ m, $z_0 = 3500$ m, $\alpha = 1.17$, and $\beta = 3.74$.	31
1.30. Mountain tallness as a function of peak elevation in the Karakoram mountains. The linear model uses eq. (1.8), with $A = 8.1$. “Model 1” uses eq. (1.7), with $z_0 = 2200$ m, and $\alpha = 5.82$. “Model 2” uses eq. (1.6), with $A = 830$ m, $z_0 = 6200$ m, $\alpha = 1.54$, and $\beta = 6.11$.	32
1.31. Mountain tallness as a function of peak elevation in the western parts of the Himalayas. The linear model uses eq. (1.8), with $A = 8.5$. “Model 1” uses eq. (1.7), with $z_0 = 1800$ m, and $\alpha = 5.18$. “Model 2” uses eq. (1.6), with $A = 670$ m, $z_0 = 5600$ m, $\alpha = 0.910$, and $\beta = 5.67$.	32
1.32. Mountain tallness as a function of peak elevation in the central parts of the Himalayas. The linear model uses eq. (1.8), with $A = 9.1$. “Model 1” uses eq. (1.7), with $z_0 = 88$ m, and $\alpha = 1.54$. “Model 2” uses eq. (1.6), with $A = 790$ m, $z_0 = 5700$ m, $\alpha = 0.808$, and $\beta = 3.83$.	33
1.33. Mountain tallness as a function of peak elevation in the eastern parts of the Himalayas. The linear model uses eq. (1.8), with $A = 11$. “Model 1” uses eq. (1.7), with $z_0 = 7.5$ m, and $\alpha = 0.940$. “Model 2” uses eq. (1.6), with $A = 700$ m, $z_0 = 5600$ m, $\alpha = 0.793$, and $\beta = 4.75$.	33
1.34. The elevation distribution (measured in area per elevation) as a function of the elevation. Data-set numbering follows the order in table 1.2.	34
1.35. Filtered noise given by eq. (1.12) with n_f given by eq. (1.16). The values of h_0 has been transformed by applying different transfer function types: Linear, exponential, and power. The parameters a and b has been chosen such that the difference in root mean square to fig. 1.35c is minimized.	36
1.36. Renderings of a landscape using the height-maps in fig. 1.35. All renderings has been shot from the same camera angle. The aspect ratio has been set to 2.4 : 1, and the horizontal field-of-view to 54.3°. For comparison with real data, see figs. 1.8 and 1.9.	37
1.37. A rendering of taking the max of figs. 1.35b and 1.35c. The aspect ratio has been set to 2.4 : 1, and the horizontal field-of-view to 54.3°. For comparison with real data, see figs. 1.8 and 1.9.	38

1. The height-map

The perhaps most important aspect when generating landscapes is the underlying *height-map*. An height-map is basically a grayscale image, where each pixel gives what the elevation above the area covered by this pixel. Since the height-map describes the topography, it dictates many aspects of a landscape such as

- Lighting conditions
- Snow or glacier coverage
- Routes of rivers
- Locations of lakes
- Vegetation coverage
- Locations of towns
- Routes of roads

1.1. Metrics of mountain ranges

In order to be able to generate realistic height-maps, it is a good idea to study some properties of height-maps representing real topography data. For this purpose, height-maps from satellite data has been collected, and the following aspects have been studied:

1. Visual appearance
2. The elevation distribution, that is, how large area¹ has as given elevation
3. The elevation gradient as a function of elevation
4. The relation between peak and valley elevation
5. The average steepness as a function of direction

The definitions and significance of items 2 to 5 are discussed in sections 1.1.1 to 1.1.4. For the source code to the programs that computes these measurements, see [1].

¹Here, “area” means the footprint covered on a smooth spheroid earth model

Table 1.1.: Mountain ranges of particular interest

Mountain range	Highest peak	Comments
Ural Mountains	Mount Narodnaya at 1900 m	Old mountains formed during late Paleozoic
Scandinavian Mountains	Galdhøpiggen at 2500 m	Highly eroded mountains formed during Paleozoic
The Alps	Mont Blanc at 4800 m	Features higher peaks and yet fertile valleys. Formed during late Mesozoic and early cenozoicum
Karakoram	K2 at 8600 m	Features high difference in elevation between peaks and valleys, and a fairly dry climate. Formed during Cenozoic. Photographies from the area shows signs of strong ongoing glacial erosion.
Himalaya	Mount Everest at 8800 m	Wetter climate than in Karakoram. Formed during Cenozoic. Slightly younger than Karakoram, and is probably still gaining height.

The input data is a raster file where the surface of the earth has been projected using a rectilinear projection of geodetic coordinates. The intensity value in each pixel encodes the elevation of that pixel. Since the coordinate system used to store the height-map will stretch the physical size of individual pixels, scaling factors has to be considered for both item 2 and item 3. A derivation of the scaling factors are found in appendix A. Another issue is that mountain ranges are seldom aligned to the coordinate system used for the raster files. This means that an image that covers an entire mountain range, must also contain other data points. To restrict what pixels can be used, a black-and-white mask has been used, where white means that the data is being considered.

The analysis has been performed on parts of the mountain ranges listed in table 1.1. To get a good coverage of different characteristics, mountain ranges of different age and elevation has been selected. Notice that there are multiple geological formations that may be called mountains including fells, stratovolcanos, and tablelands. For this study, only mountains formed by means of uplift or deformation as a result of collisions between tectonic plates, and erosion, have been considered. Thus, the term *mountain* in this text is restricted to that meaning. This means that a fell may be a mountain (and usually is, except on Iceland). Mont Blanc is a mountain, but Mount Elbrus, or Mount Vesuvius is not.

For practical reasons, the largest mountain ranges has been split in parts. The split has been done with only the height-map as reference. Thus, it is possible that the partitioning used within this paper does not correspond to partitioning commonly used in geology. The partitioning used within this paper is presented in table 1.2.

Table 1.2.: The partitioning used for data analysis

Mountain range partition	Description
Northern Ural Mountains	From the at the arctic ocean to Shchekur'ya
Southern Ural Mountains	From Shchekur'ya to Perm
Northern Scandinavian Mountains	From Narvik to Trondheim
Southern Scandinavian Mountains	From Trondheim down to the bottom of the Norwegian Head
The Alps	Not partitioned
Karakoram	Not partitioned
Western Himalayas	The western parts stretches from Nanga Parbat in the west, to Dhaulagiri in the east. The area also includes the Kashmir valley, to the south of Nanga Parbat.
Central Himalayas	The central parts stretches from the Annapurna massif in the west, to Kanchenjunga in the east
Eastern Himalayas	Everything to the east of Kanchenjunga

1.1.1. The elevation distribution

To compute the elevation distribution, a linear histogram with a bucket size of 32 m is used. For each pixel, the corresponding area is accumulated in the corresponding bucket. The area is given by eq. (A.5), with $l = 0$ and $m = 0$. To get the area per elevation, the value in each bucket is divided by its size, that is 32 m.

1.1.2. The elevation gradient

The gradient as a function the of elevation is interesting because it indicates how the steepness at a given location depends on its elevation. Let x be any horizontal coordinate. Then, the function is the right hand side of the differential equation

$$\frac{dz}{dx} = f(z) \quad (1.1)$$

with solutions

$$z(x) = \left[\int \frac{1}{f(z)} dz - C \right]^{-1}(x) = \left\{ t = \frac{z}{z_0} \right\} = \left[z_0 \int \frac{1}{f(t)} dt - C \right]^{-1}(x) \quad (1.2)$$

Equation (1.2) then gives an elevation profile.

The elevation and slope may vary over large magnitudes, which motivates the use of logarithmic diagrams. Also, the slope is defined by the “climb” over “run” ratio and, since $\log(a : b) = \log(a) - \log(b)$, using a logarithm equalizes the ratio with its inverse.

To use eq. (1.1) or eq. (1.2) when synthesizing terrain, it useful to fit the measurements to a smooth function. It is reasonable to assume that $f(0) = 0$, since

the sea is assumed to be flat². The simplest model that fulfils this criterium is a power function, i.e

$$f(z) = \left(\frac{z}{z_0}\right)^\alpha, \alpha \neq 0. \quad (1.3)$$

Then, from eq. (1.2)

$$\begin{cases} z(x) = z_0 \exp\left(\frac{x+C}{z_0}\right) & , \alpha = 1 \\ z(x) = z_0 \left(\frac{(x+C)(1-\alpha)}{z_0}\right)^{1/(1-\alpha)} & , \alpha \neq 1 \end{cases} \quad (1.4)$$

For $\alpha = 1$, $z(x)$ becomes an exponential. Otherwise, it is a translated power function. If $\alpha < 1$, the exponent is greater than 1 and $z(x)$ grows like a polynomial. When $\alpha > 1$, the exponent becomes negative and there is a singularity when $x = -C$.

A more elaborate model, is a multi-mode model, which can describe differences between low and high terrain. One such model is

$$\frac{dz}{dx} = A \cdot \frac{(z/z_0)^\alpha}{1 + (z/z_0)^\alpha} \cdot \frac{1 + (z/z_0)^{2\beta}}{1 + (z/z_0)^\beta} \quad (1.5)$$

where α is used for the low terrain, and β is used for the high terrain. The value of z_0 determines the transition elevation.

It is possible that the input data contains far more low points than it contains high points. Thus, to not overweight data for certain elevations, measurements have been grouped by the elevation into a histogram with bucket size $2^{k/12}$ m, where $k \in [0, 159]$. Then, N different randomly selected data-points have been taken from each bucket individually, to be considered for analysis. To fit model parameters `curve_fit` from `scipy`[2] has been used, with the start values listed and constraints listed in table 1.3, and table 1.4.

1.1.3. The relation between peak and valley elevation

A peak can have a high elevation because its base is already at a high elevation, or the actual peak is tall. It is then natural to define the *tallness* of a mountain as the difference in elevation between the peak and the base. All such combinations are shown in fig. 1.1. This is related to the relation between peak and valley elevations: A region with low and tall mountains will show a larger difference in elevation between peaks and valleys than a region with high and short mountains. Another way of thinking of this is individual peaks located on a larger curved structure. In one dimension, this would behaviour would be reproduced by

$$z = f(x) \cdot (a + b \sin^2(kx/2))$$

, where b and a would be measurements of peak and valley elevations. A small a compared b would produce low and tall mountains, and vice versa.

²“Flat” here means absence of topographic features

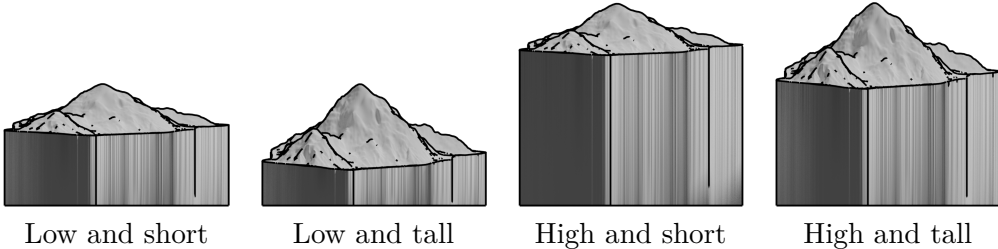


Figure 1.1.: The same mountain but with different “tallness”. The low two versions classified as “low”, both have the same peak elevation, but the tall one, is considerably steeper. Also, the two versions marked as “high” shares peak elevation. The tall mountains have the same gradient, but not the same peak elevation.

For a (finite) sequence, it is easy to find all peaks and valleys. For the peaks, keep track of whether or not the current value is greater than or equal to previous value. When this is false, save the previous value as a peak. Now, continue until the current value is greater than previous value. When it is, save the previous value as a valley. This will generate one sequence of peaks, and one sequence of valleys. With interpolation it is then possible to plot tallness as a function of elevation. More precisely, for every local maxima, use the interpolated value between the two closest local minima as the elevation of the corresponding valley.

For two-dimensional data, such as height-maps, a location can be a peak in one direction, and a valley in the other direction. This is called a saddle point and should not count as a peak or a valley. While a local extremum should be a requirement for a peak, the same requirement for valleys may be too restrictive, because most valleys will be curves rather than points. Thus, a better approach is to pick N cross-sections at random, and then use the one-dimensional peak-valley detector.

When collecting data, the fact that the elevation may not be uniform must be considered. Thus, same same histogram as in section 1.1.2 has been used, but instead of elevation-gradient pairs, each bucket contains peak-valley elevation pairs. To fit data points to a curve, an expression similar to the right hand side of eq. (1.5) has been used, that is

$$\text{tallness} = A \cdot \frac{(z/z_0)^\alpha}{1 + (z/z_0)^\alpha} \cdot \frac{1 + (z/z_0)^{2\beta}}{1 + (z/z_0)^\beta} \quad (1.6)$$

For comparison, a pure power law

$$\text{tallness} = A \cdot (z/z_0)^\alpha \quad (1.7)$$

is also tested³, as well as a linear model

$$\text{tallness} = \frac{z}{A} \quad (1.8)$$

³The parameter A in eq. (1.7) exists only to make the expression dimension-full. Its value is always 1, but it has the dimension of length.

Table 1.3.: Initial values for model parameters

Equation	A	z_0	α	β
eq. (1.3)		4096 m	0.5	
eq. (1.5)	0.5	256 m	2	0.25
eq. (1.7)		128 m	2	
eq. (1.6)	2048 m	1024 m	2	0.25

Table 1.4.: Constraints on model parameters

Equation	A	z_0	α	β
eq. (1.3)		$[0, \infty[$	$[0, 1[$	
eq. (1.5)	$[0, \infty[$	$[0, \infty[$ m	$[0, \infty[$	$[0, 1[$
eq. (1.7)		$[0, \infty[$	$[0, \infty[$	
eq. (1.6)	$[0, \infty[$ m	$[0, \infty[$ m	$[0, \infty[$	$[0, \infty[$

1.1.4. The average steepness as a function of direction

It is possible that a mountain range have an anisotropic behaviour in steepness. For example, the hills may be steep when looking from west, but flat when looking from east. A direction with a maximum in steepness is here after called a *scarp direction*.

One way of measuring the directional dependency in steepness is to define a horizontal direction, that represents the direction vector projected on to the horizontal plane, from the current face to an imaginary camera.

$$\mathbf{d}_{xy} = -\sin(\theta)\hat{\mathbf{x}} + \cos(\theta)\hat{\mathbf{y}} \quad (1.9)$$

The angle θ has been chosen to reflect the convention that 0 maps to north, and $\pi/2$ maps to east. Then consider the the normal vector of a perfect scarp, facing in the same horizontal direction as the actual hill. Its normal vector is then

$$\mathbf{n}_{xy} = \frac{n_x \hat{\mathbf{x}} + n_y \hat{\mathbf{y}}}{\sqrt{n_x^2 + n_y^2}} \quad (1.10)$$

, where n_x and n_y are the horizontal components of the actual normal vector. Now define the average steepness in the direction of θ as

$$\bar{S}(\theta) = \frac{1}{M} \int \max(\mathbf{n} \cdot \mathbf{d}_{xy}, 0) dA \quad (1.11)$$

, where

$$M = \int \max(\mathbf{n}_{xy} \cdot \mathbf{d}_{xy}, 0) dA$$

With this definition $\bar{S}(\theta)$ will be equal to one, if every hill in the direction of θ is a perfect scarp.

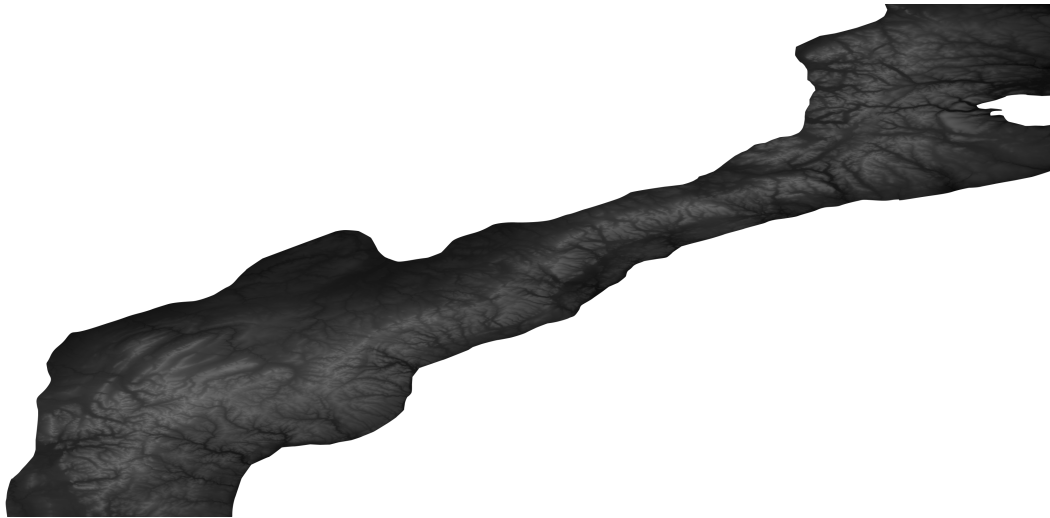


Figure 1.2.: Height-map showing the elevation of the northern parts of the Ural mountains, retrieved from [3]. For partitioning, see table 1.2. © DLR e.V. (2014-2018) and © Airbus Defence and Space GmbH 2022 provided under COPERNICUS by the European Union and ESA; all rights reserved.

From eq. (1.10), it is clear that the definition is ill-formed if the normal vector has no horizontal component, because the presence of an indeterminate form, in this case $\frac{0}{0}$. To avoid this degenerate case, pixels where the horizontal component of the normal vector is less than 2^{-16} are ignored. To sample values of $\bar{S}(\theta)$, $\Delta\theta = \frac{\pi}{32}$ is used as step size.

1.2. Measurements of real mountain ranges

1.2.1. Visual comparisons

Height-maps for the mountain ranges listed table 1.1 are presented in figs. 1.2 to 1.7 and 1.10 to 1.12. These images are all uncompensated for the earth curvature, which implies that regions at a high latitude are heavily distorted. Nevertheless, many features can be spotted by visual inspection. Notably, the ridges and valleys forms tree-like, fractal structures.

The Ural mountains

Height-maps of the Ural mountains are shown in figs. 1.2 and 1.3, A characteristic of the Ural mountains is the abrupt change in direction from north to north-east. The southern parts is almost aligned with the longitudes, while the northern parts runs north-east. The highest peak is located in southern part of the northern parts, from which the elevation decays towards the arctic coast. From fig. 1.3 and fig. 1.2 it is clear that the northern parts shows a larger fraction of perpendicular valleys,

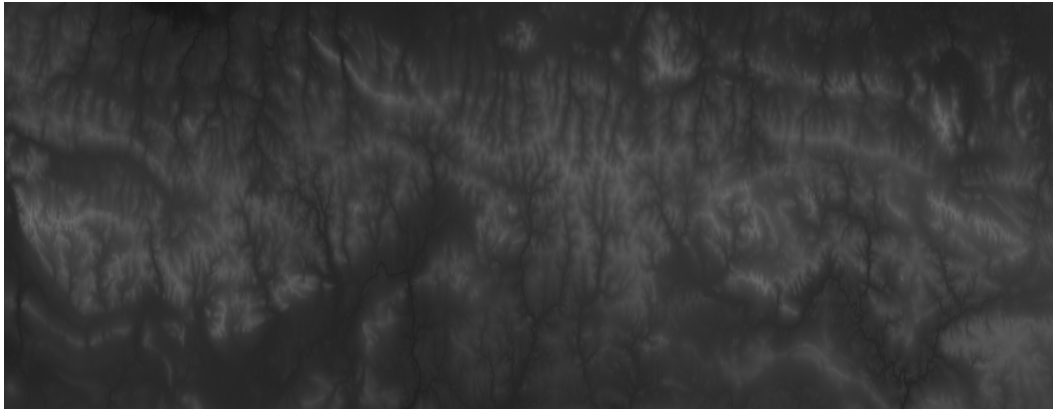


Figure 1.3.: Height-map showing the elevation of the southern parts of the Ural mountains, retrieved from [3]. For partitioning, see table 1.2. In order to save space, this height-map is oriented from north-south, rather than west-east. Since this part of the Ural mountains runs in the north direction and the latitude is quite high, the mountains appear stretched in the west-east direction. © DLR e.V. (2014-2018) and © Airbus Defence and Space GmbH 2022 provided under COPERNICUS by the European Union and ESA; all rights reserved.

than the southern parts, where parallel valleys are also visible.

The Scandinavian mountains

Height-maps for the Scandinavian mountains are shown in figs. 1.4 and 1.5. In the west, the Scandinavian mountains drop straight into the sea, without no or very thin shore-lines. The waterline forms large valley systems, where in the southern parts, the water almost touches the walls of the highest peaks. To the east, long valleys run down from the mountains. Other than that, the topography is washed out, though it is possible to spot Galdhøpiggen as separated from Glittertind.

The Alps

A height-map for the Alps is shown in fig. 1.6. The range runs mainly in the west-east direction, and curls to the west. Its highest peaks are located in the west, and in the middle (measured perpendicular to the main curve). Notable peaks in this region includes Mont Blanc, Monte Rosa, and Matterhorn, the latter being located closer to the southern boundary. To the east of the highest peaks, the elevation appears to be quite uniform, but decays slowly. Long valleys run in parallel to the ridges. Also, there are four valleys that crosses the entire range, which meet in the north-middle.

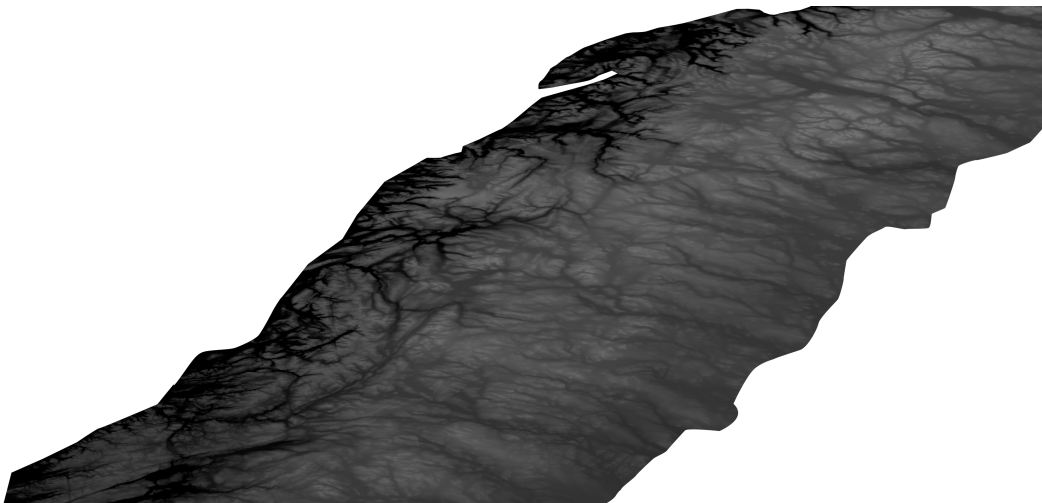


Figure 1.4.: Height-map showing the elevation of the northern parts of the Scandinavian mountains, retrieved from [3]. For partitioning, see table 1.2. © DLR e.V. (2014-2018) and © Airbus Defence and Space GmbH 2022 provided under COPERNICUS by the European Union and ESA; all rights reserved.

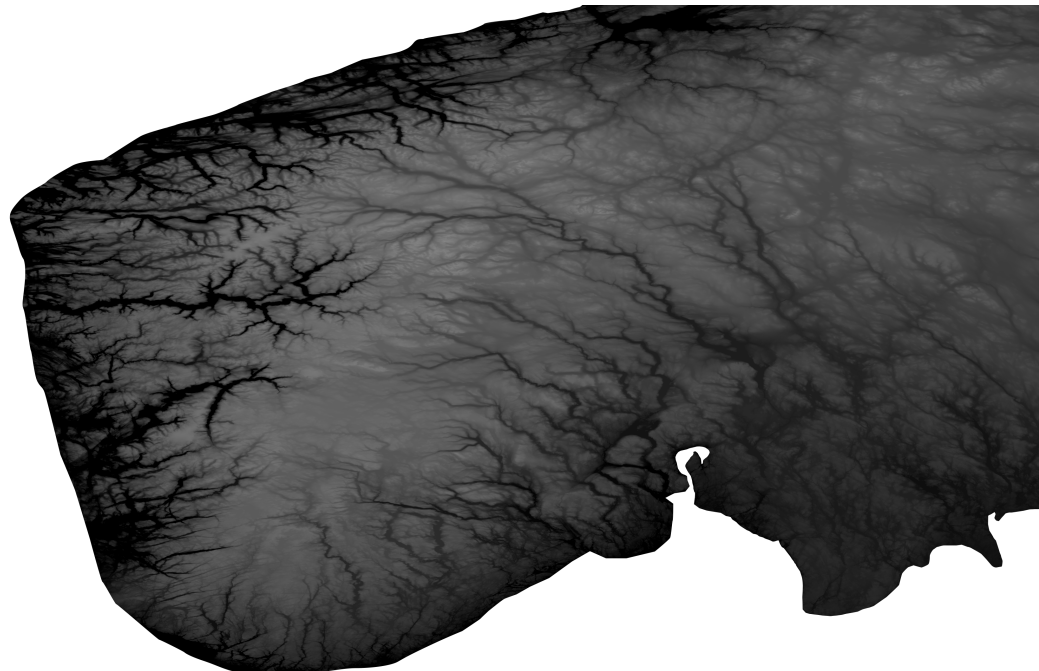


Figure 1.5.: Height-map showing the elevation of the southern parts of the Scandinavian mountains, retrieved from [3]. For partitioning, see table 1.2. © DLR e.V. (2014-2018) and © Airbus Defence and Space GmbH 2022 provided under COPERNICUS by the European Union and ESA; all rights reserved.



Figure 1.6.: Height-map showing the elevation of the Alps, retrieved from [3]. © DLR e.V. (2014-2018) and © Airbus Defence and Space GmbH 2022 provided under COPERNICUS by the European Union and ESA; all rights reserved.

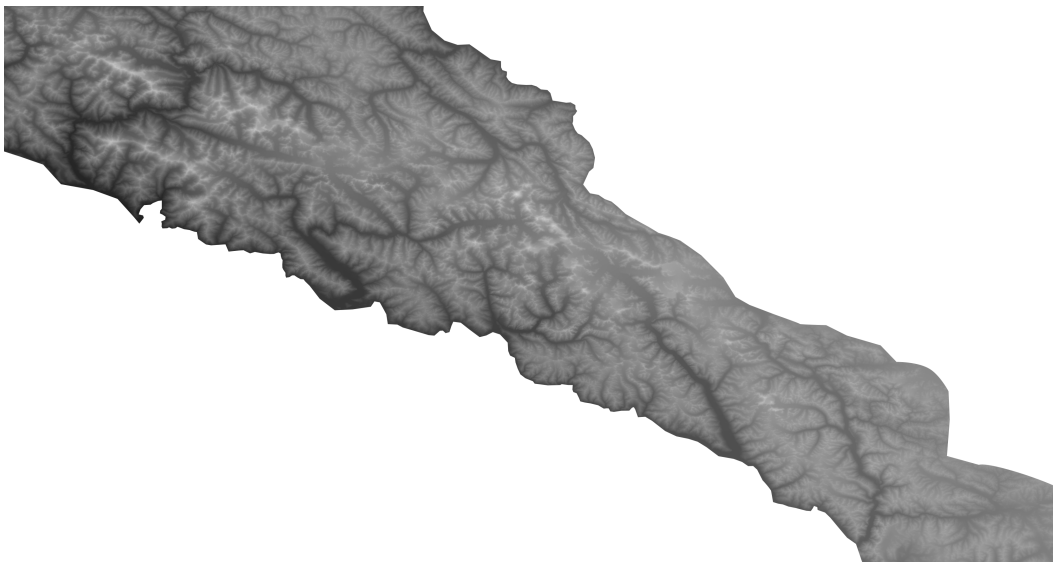


Figure 1.7.: Height-map showing the elevation in the Karakoram mountains, retrieved from [3]. © DLR e.V. (2014-2018) and © Airbus Defence and Space GmbH 2022 provided under COPERNICUS by the European Union and ESA; all rights reserved.

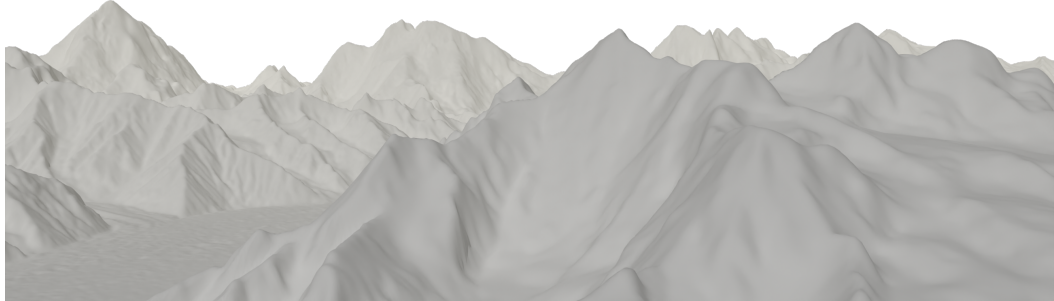


Figure 1.8.: A rendering from the north ridge of Masherbrum towards north-east, using a scale-corrected portion of fig. 1.7 as height-map. The aspect ratio has been set to 2.4 : 1, and the horizontal field-of-view to 54.3°

The Karakoram mountains

A height-map of the Karakoram mountains is shown in fig. 1.7. Here there are four distinct regions of high mountains. In north-east, there is Batura Sar. On the opposite side of the valley is Disteghil Sar. To the south of these massifs is Rakaposhi. Moving east-south-east there is a bunch of scattered high peaks, which includes K2, and the Gasherbrums. Like in the Alps, there are long valleys that runs parallel to the ridges. Compared to the Alps, the valleys are relatively wider.

The Himalayas

Throughout the whole range, the southern front has a low elevation, while the northern front has a high elevation. Compared to the Karakoram, valleys in the Himalayas tend to be relatively narrower. Also, the main valleys goes more perpendicular to the ridges.

The height-map for the western parts of the Himalayas is shown in fig. 1.10. A notable feature here is the Kashmir valley, located south of Nanga Parbat. Except for Nanga Parbat, there are not many outstanding peaks within this area. The peaks becomes higher and more separated in the south-east, where Dhaulagiri is located. Again, a prominent peak. More interestingly, there is an isolated peak in the south, right at the border to the Tibetan plateau.

When moving south-east to the central parts of the Himalayas shown in fig. 1.11, the valleys becomes narrow and deep. To the south south, where the Indian sub-continent lies, the valleys join to a valley that runs in parallel to the ridges. The area features large and high massifs. The largest being Annapurna, and the highest being Mount Everest-Lhotse.

Further east (see fig. 1.12), the Himalayas bend towards the north, and meets

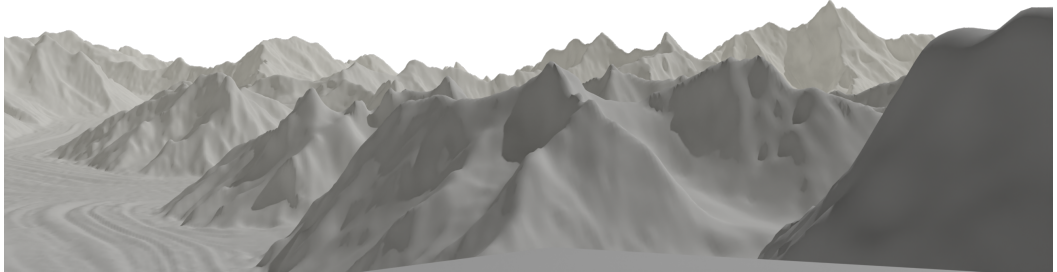


Figure 1.9.: A rendering from the south face of K2 towards south-west, using a scale-corrected portion of fig. 1.7 as height-map. The aspect ratio has been set to 2.4 : 1, and the horizontal field-of-view to 54.3°

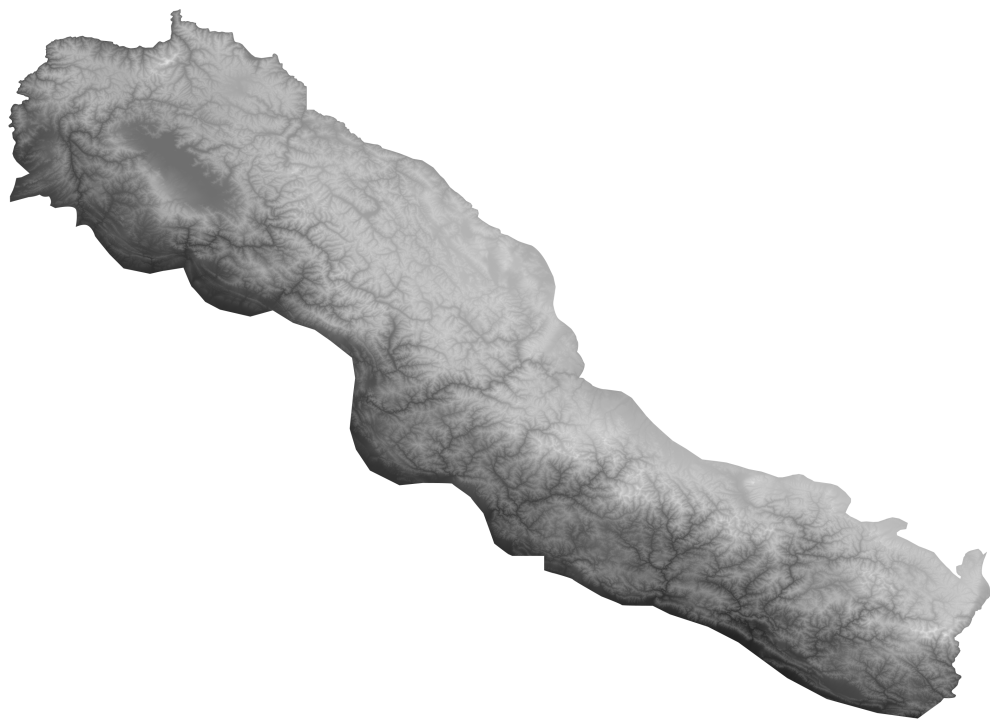


Figure 1.10.: Height-map showing the elevation in the western parts of the Himalayas, retrieved from [3]. For partitioning, see table 1.2 © DLR e.V. (2014-2018) and © Airbus Defence and Space GmbH 2022 provided under COPERNICUS by the European Union and ESA; all rights reserved.

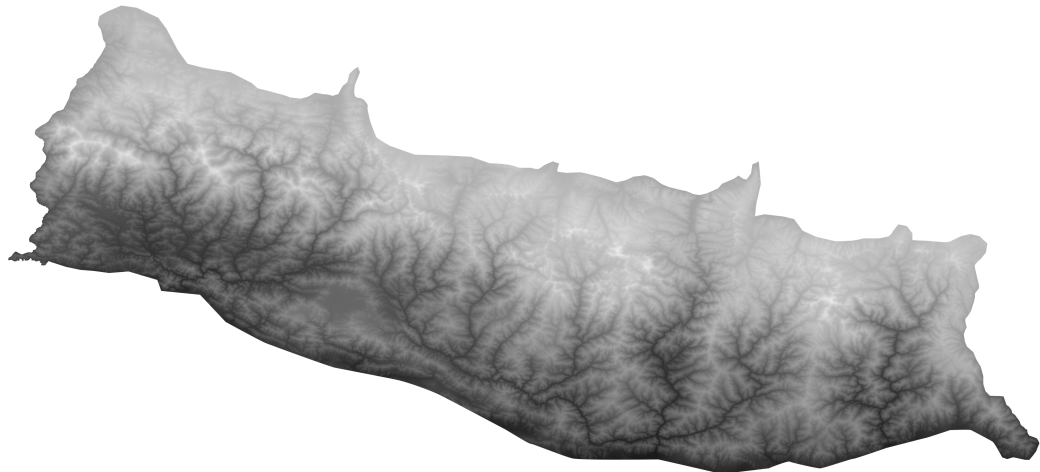


Figure 1.11.: Height-map showing the elevation in the central parts of the Himalayas, retrieved from [3]. For partitioning, see table 1.2. © DLR e.V. (2014-2018) and © Airbus Defence and Space GmbH 2022 provided under COPERNICUS by the European Union and ESA; all rights reserved.



Figure 1.12.: Height-map showing the elevation in the eastern parts of the Himalayas, retrieved from [3]. For partitioning, see table 1.2. © DLR e.V. (2014-2018) and © Airbus Defence and Space GmbH 2022 provided under COPERNICUS by the European Union and ESA; all rights reserved.

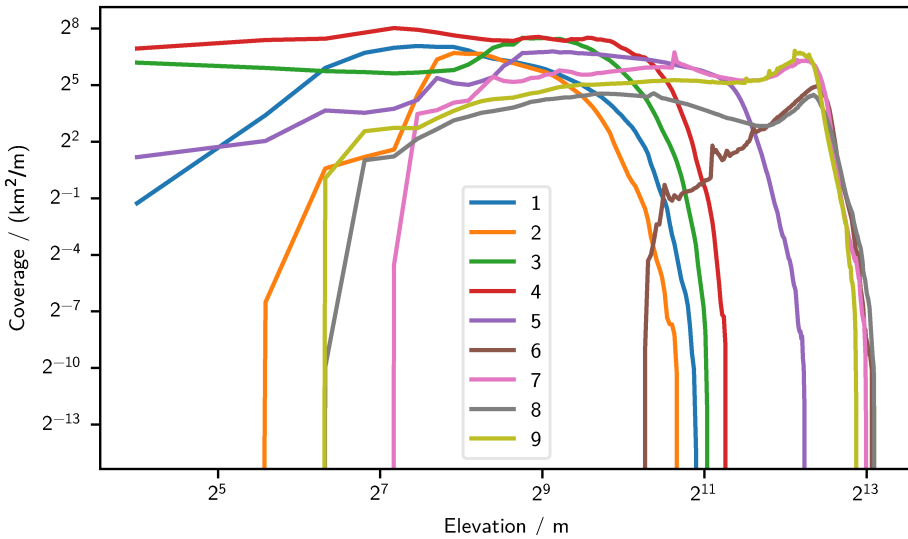


Figure 1.13.: The elevation distribution (measured in area per elevation) as a function of the elevation. Data-set numbering follows the order in table 1.2.

up with a couple of smaller sub-ranges where the major valleys are parallel to the mountain ridges.

1.2.2. The elevation distribution

The elevation distributions for the data-sets listed in table 1.2 are shown in 1.13. The figure shows that the elevation coverage has a small growth for low elevations, and a fast for roll-off higher elevations. In between, there is a maximum coverage. Thus, the elevation is not uniformly distributed. By inspection, some data-sets also have a low-elevation cutoff. In particular, the measurements for the Karakoram mountains start above 1000 m. This is because these data-sets cover high-based mountain ranges, whereas the other ones have their lowest base close to sea-level.

1.2.3. The gradient as a function of the elevation

The gradient as a function of elevation for the mountain ranges listed table 1.1 is presented in figs. 1.14 to 1.23. From these figures it is clear that an exponential growth model does not work. At least if the slope at sea-level is forced to zero. It underestimates the steepness of the lowest peaks, or overestimates the steepness of the highest peaks. The model described by eq. (1.5) is in general a good fit, though it is clear that it may be either convex or concave depending on the input data. If eq. (1.5) is too complicated⁴, eq. (1.3) with $\alpha < 1$ also works. As shown in fig. 1.14, $\alpha \approx 1/3$ should in general be a good value. From eq. (1.4), this gives a power law with the exponent 3/2.

1.2.4. The relation between peak and valley elevation

Figures 1.24 to 1.33 shows the relation between peak elevation and tallness. As with the gradient, the tallness increases with elevation. fig. 1.24 shows that, in general, the dependency is sub-linear for lower peaks, and super-linear for higher peaks. The transition elevation appears around 5600 m. This kink shows up in figs. 1.30 to 1.33, and is probably related to the fact that there are no valleys with elevation higher than 5000 m to 6000 m, yet there are peaks with an elevation up to more than 8000 m. Thus, these high mountains has to be tall.

A high-elevation kink is also visible in the curve fits for the Alps and the Ural mountains, though in this case it is possible that this is an artefact from changing parameters in eq. (1.6). From figs. 1.24 to 1.29, it is clear that a sub-linear model works quite well for lower peaks⁵. By the curve-fits in these figures, it is clear that a single-exponent model such as eq. (1.7), requires a higher exponent for a higher mountain range. In particular, the profile for northern parts of the Scandinavian mountains (see fig. 1.27) is described with $\alpha = 0.889$ while the Alps (see fig. 1.29), require $\alpha = 1.12$, which is slightly above linear. It should be mentioned that for the Alps, a pure linear model is also a good fit.

⁴Solving eq. (1.5) would in general require numerical methods in at least some stage of the process
⁵“Low” here means an elevation less than 5000 m

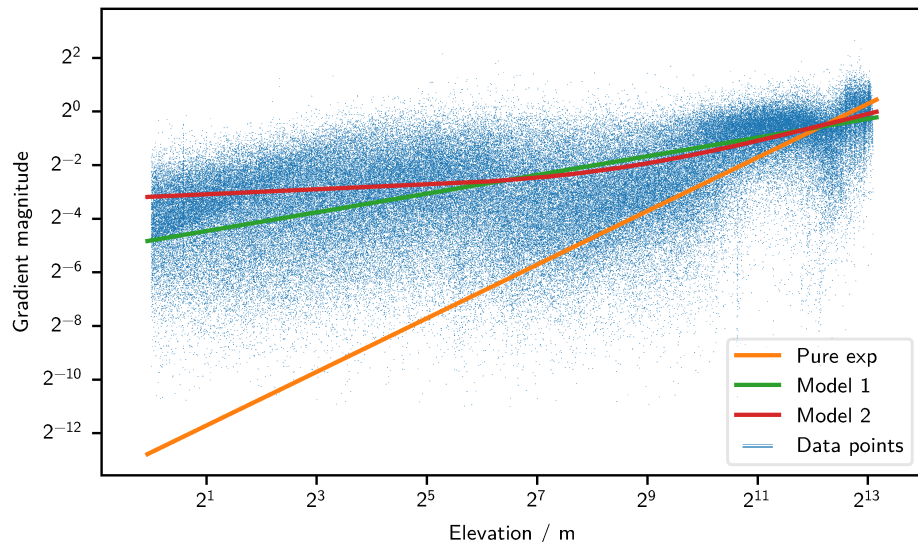


Figure 1.14.: The gradient as a function of elevation with all data-sets considered. “Model 1” uses eq. (1.3), with $z_0 = 14\,000$ m and $\alpha = 0.349$. “Model 2” uses eq. (1.5), with $A = 0.45$, $z_0 = 330$ m, $\alpha = 0.178$, and $\beta = 0.417$

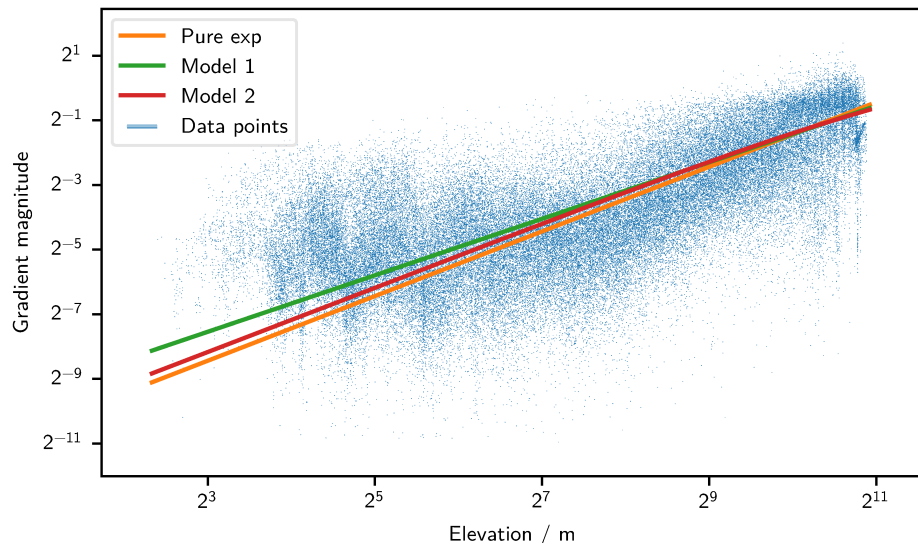


Figure 1.15.: The gradient as a function of elevation in the northern parts of the Ural mountains. “Model 1” uses eq. (1.3), with $z_0 = 3200$ m and $\alpha = 0.874$. “Model 2” uses eq. (1.5), with $A = 1.7$, $z_0 = 2900$ m, $\alpha = 1.02$, and $\beta = 0.282$

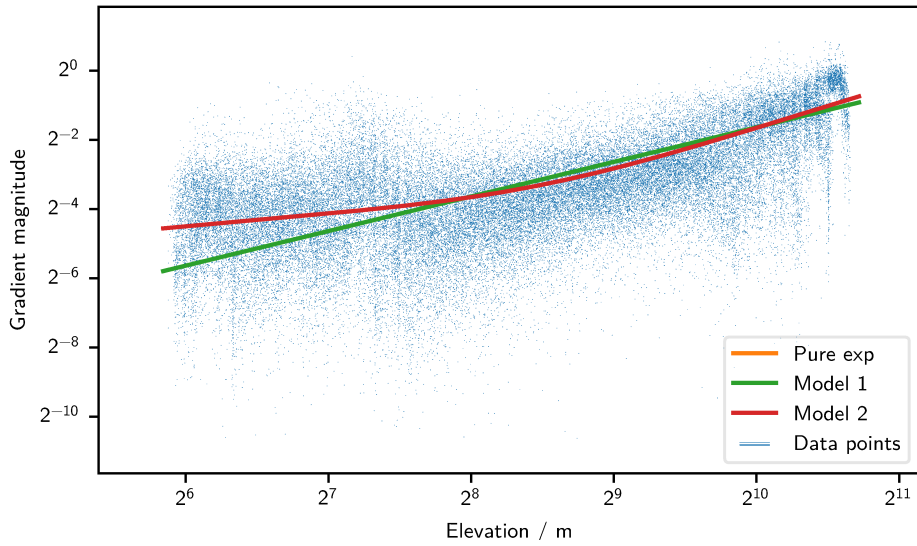


Figure 1.16.: The gradient as a function of elevation in the southern parts of the Ural mountains. “Model 1” uses eq. (1.3), with $z_0 = 3200$ m, and $\alpha = 1$. “Model 2” uses eq. (1.5), with $A = 0.20$, $z_0 = 360$ m, $\alpha = 0.634$, and $\beta = 1$.

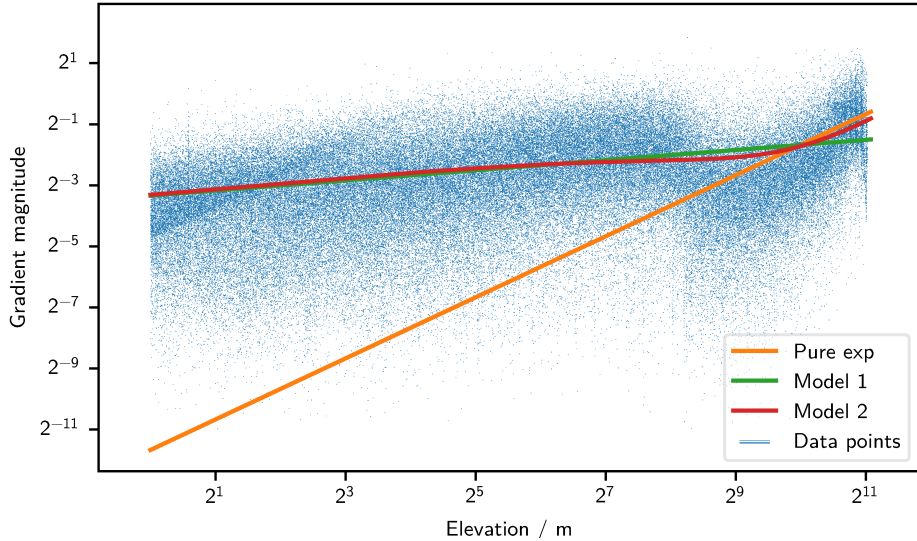


Figure 1.17.: The gradient as a function of elevation in the northern parts of the Scandinavian mountains. “Model 1” uses eq. (1.3), with $z_0 = 1\,100\,000$ m, and $\alpha = 0.166$. “Model 2” uses eq. (1.5), with $A = 0.62$, $z_0 = 1100$ m, $\alpha = 0.236$, and $\beta = 1$

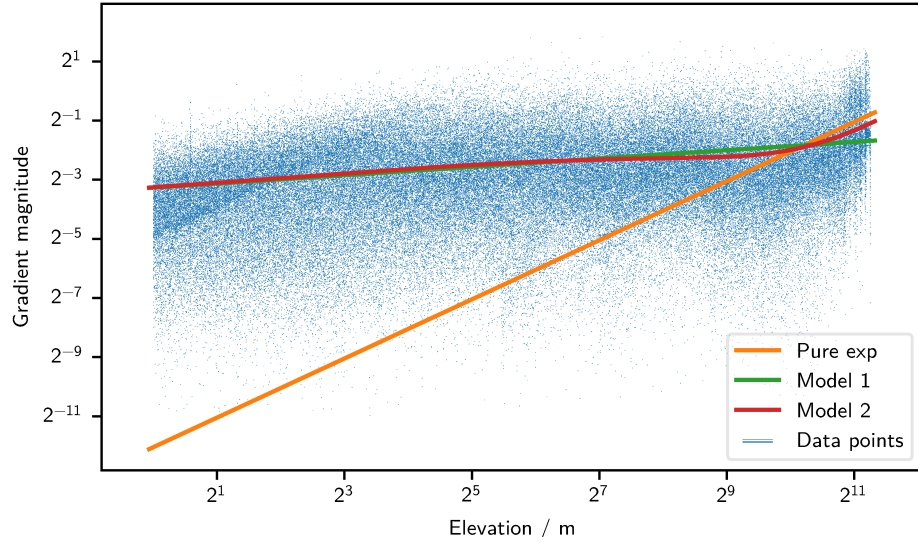


Figure 1.18.: The gradient as a function of elevation in the southern parts of the Scandinavian mountains. “Model 1” uses eq. (1.3), with $z_0 = 9\,900\,000$ m, and $\alpha = 0.141$. “Model 2” uses eq. (1.5), with $A = 0.21$, $z_0 = 1300$ m, $\alpha = 0.208$, and $\beta = 1$.

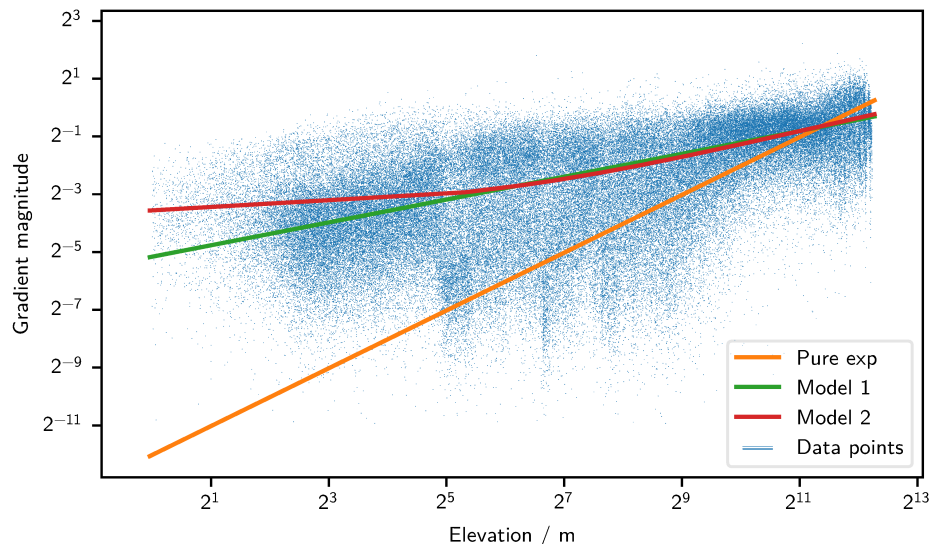


Figure 1.19.: The gradient as a function of elevation in the Alps. “Model 1” uses eq. (1.3), with $z_0 = 8500$ m, and $\alpha = 0.395$. “Model 2” uses eq. (1.5), with $A = 0.30$, $z_0 = 68$ m, $\alpha = 0.169$, and $\beta = 0.371$.

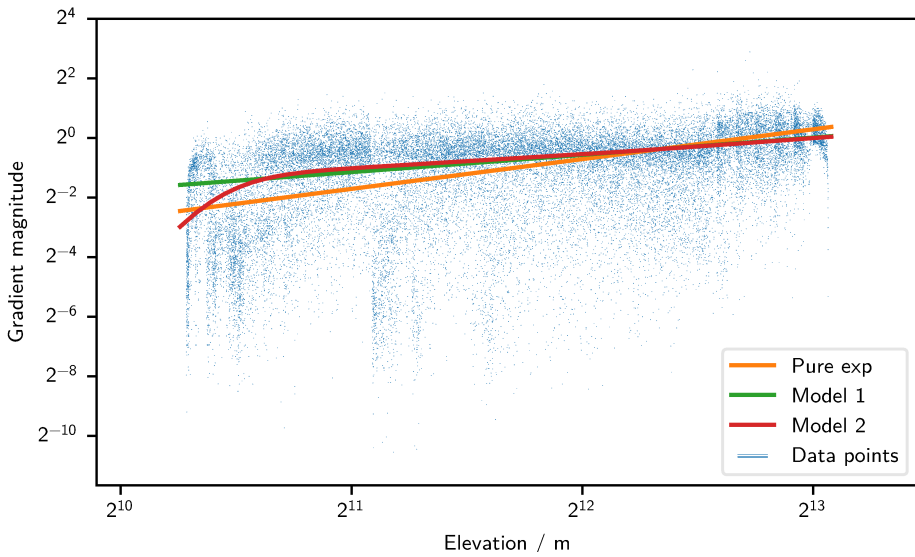


Figure 1.20.: The gradient as a function of elevation in the Karakoram mountains. “Model 1” uses eq. (1.3), with $z_0 = 8000$ m, and $\alpha = 0.580$. “Model 2” uses eq. (1.5), with $A = 0.44$, $z_0 = 1300$ m, $\alpha = 9.67$, and $\beta = 0.559$.

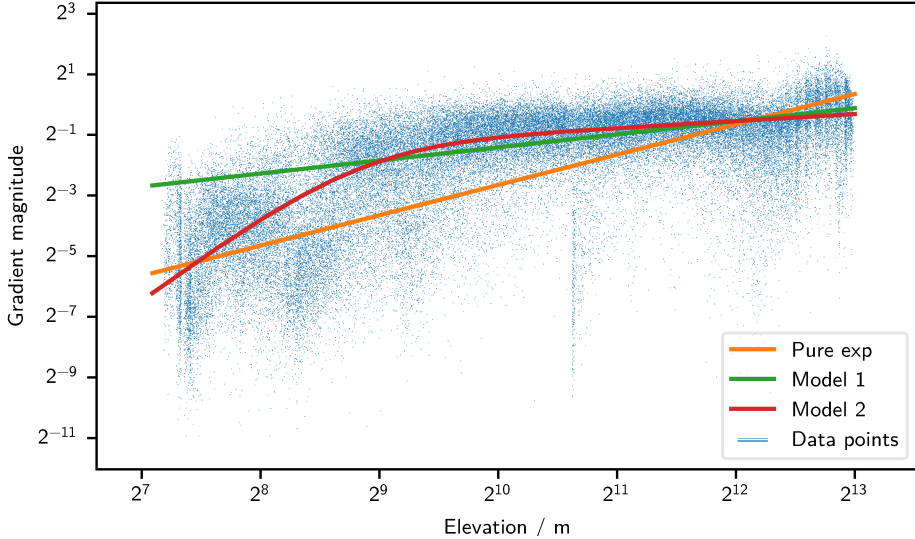


Figure 1.21.: The gradient as a function of elevation in the western parts of the Himalayas. “Model 1” uses eq. (1.3), with $z_0 = 9900$ m, and $\alpha = 0.432$. “Model 2” uses eq. (1.5), with $A = 0.46$, $z_0 = 460$ m, $\alpha = 2.80$, and $\beta = 0.257$.

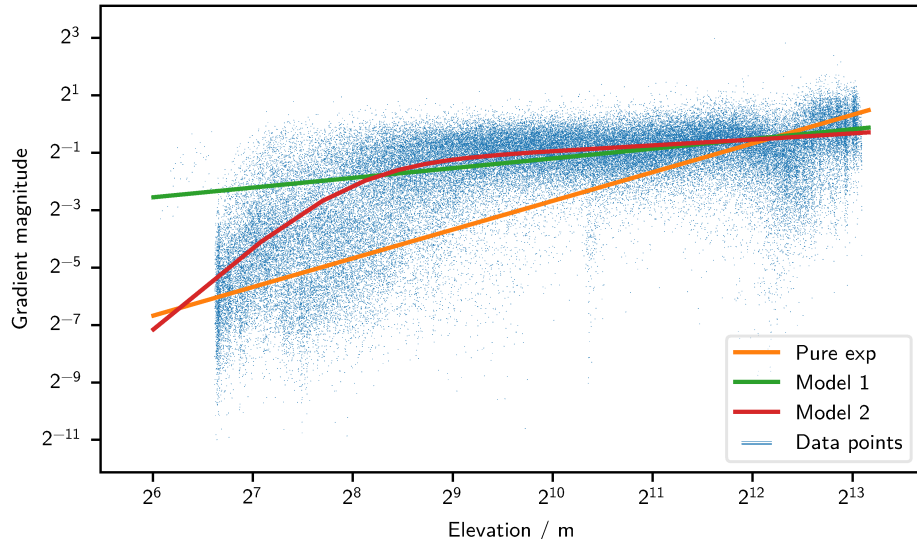


Figure 1.22.: The gradient as a function of elevation in the central parts of the Himalayas. “Model 1” uses eq. (1.3), with $z_0 = 12\,000$ m, and $\alpha = 0.339$. “Model 2” uses eq. (1.5), with $A = 0.43$, $z_0 = 250$ m, $\alpha = 2.94$, and $\beta = 0.230$.

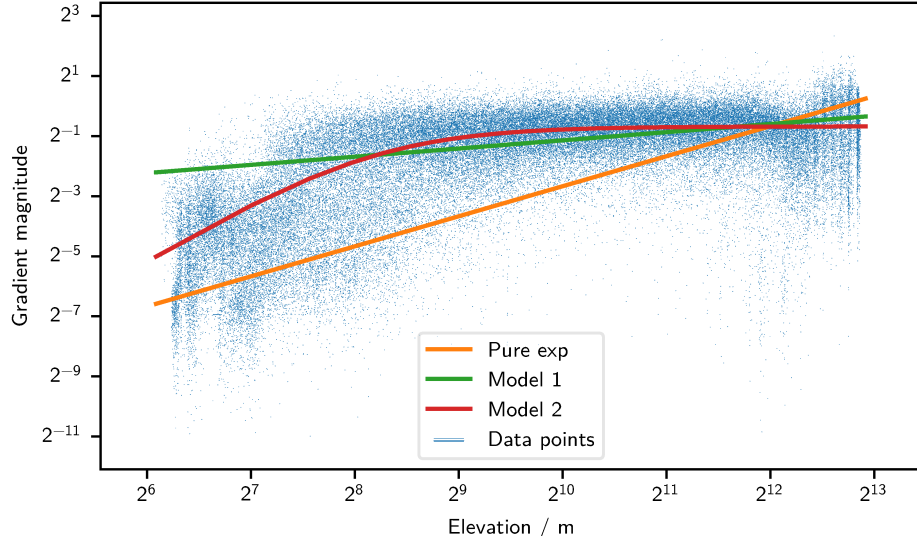


Figure 1.23.: The gradient as a function of elevation in the eastern parts of the Himalayas. “Model 1” uses eq. (1.3), with $z_0 = 19\,000$ m, and $\alpha = 0.272$. “Model 2” uses eq. (1.5), with $A = 0.625$, $z_0 = 290$ m, $\alpha = 2.06$, and $\beta = 0$.

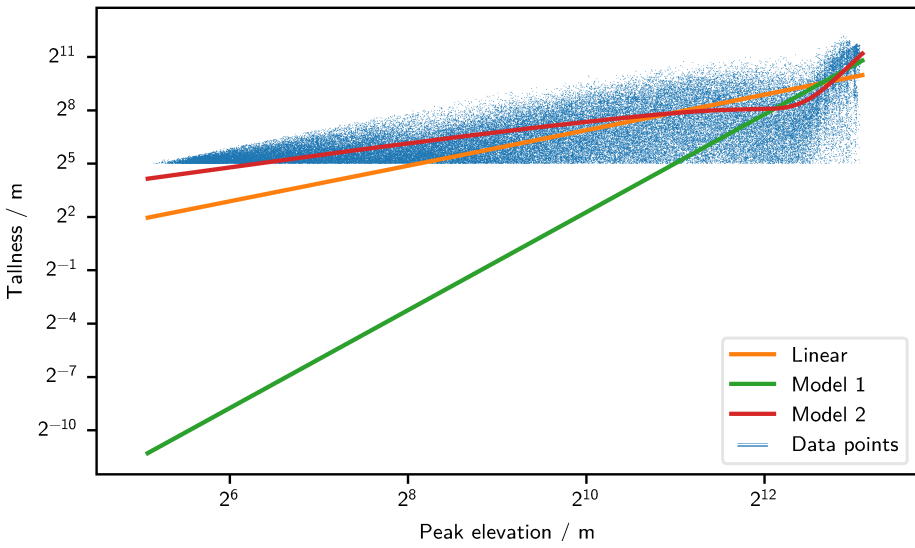


Figure 1.24.: Mountain tallness as a function of peak elevation with all data-sets considered. The linear model uses eq. (1.8), with $A = 8.7$. “Model 1” uses eq. (1.7), with $z_0 = 580$ m, and $\alpha = 2.75$. “Model 2” uses eq. (1.6), with $A = 720$ m, $z_0 = 5600$ m, $\alpha = 0.719$, and $\beta = 4.06$.

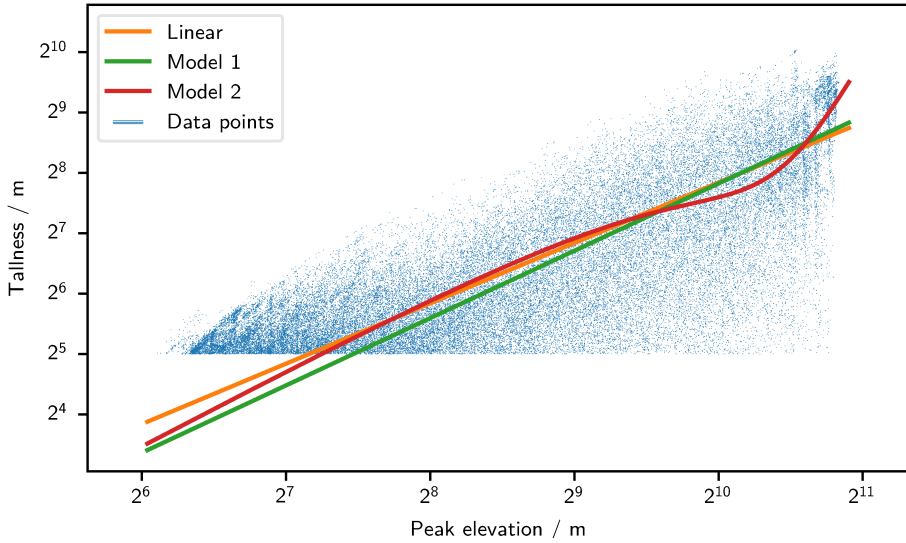


Figure 1.25.: Mountain tallness as a function of peak elevation in the northern parts of the Ural mountains. The linear model uses eq. (1.8), with $A = 4.5$. “Model 1” uses eq. (1.7), with $z_0 = 7.9$ m, and $\alpha = 1.11$. “Model 2” uses eq. (1.6), with $A = 590$ m, $z_0 = 1400$ m, $\alpha = 1.27$, and $\beta = 3.21$.

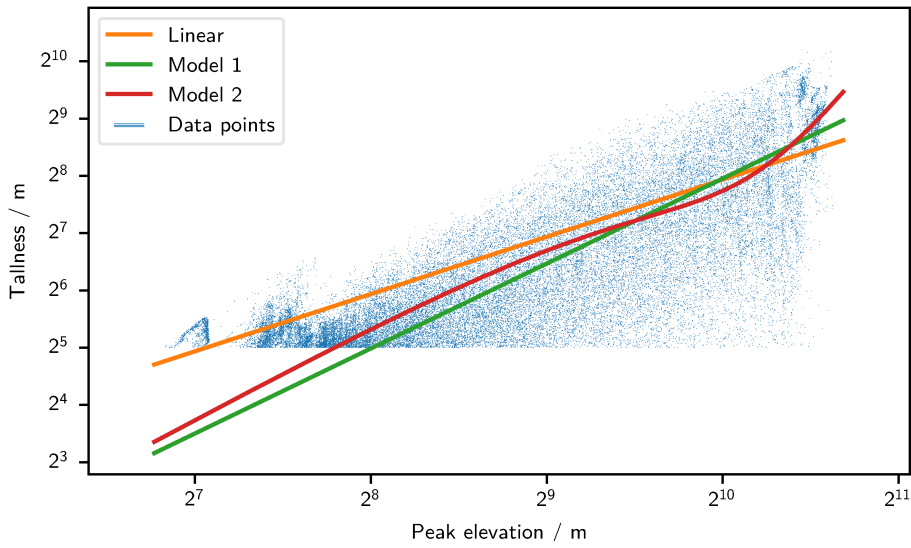


Figure 1.26.: Mountain tallness as a function of peak elevation in the southern parts of the Ural mountains. The linear model uses eq. (1.8), with $A = 4.2$. “Model 1” uses eq. (1.7), with $z_0 = 25$ m, and $\alpha = 1.48$. “Model 2” uses eq. (1.6), with $A = 590$ m, $z_0 = 1200$ m, $\alpha = 1.67$, and $\beta = 2.85$.

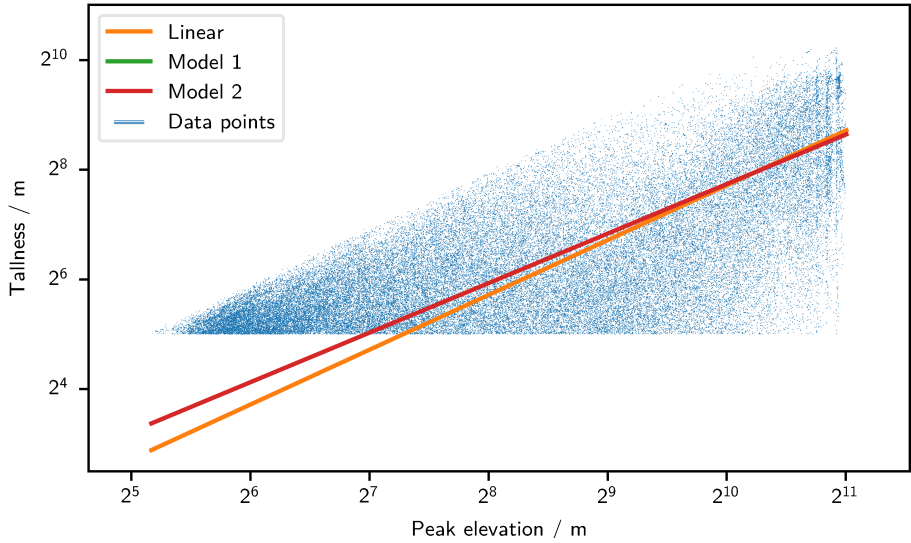


Figure 1.27.: Mountain tallness as a function of peak elevation in the northern parts of the Scandinavian mountains. The linear model uses eq. (1.8), with $A = 4.9$. “Model 1” uses eq. (1.7), with $z_0 = 2.71$ m, and $\alpha = 0.904$. “Model 2” uses eq. (1.6), with parameters that makes it almost identical to Model 1.

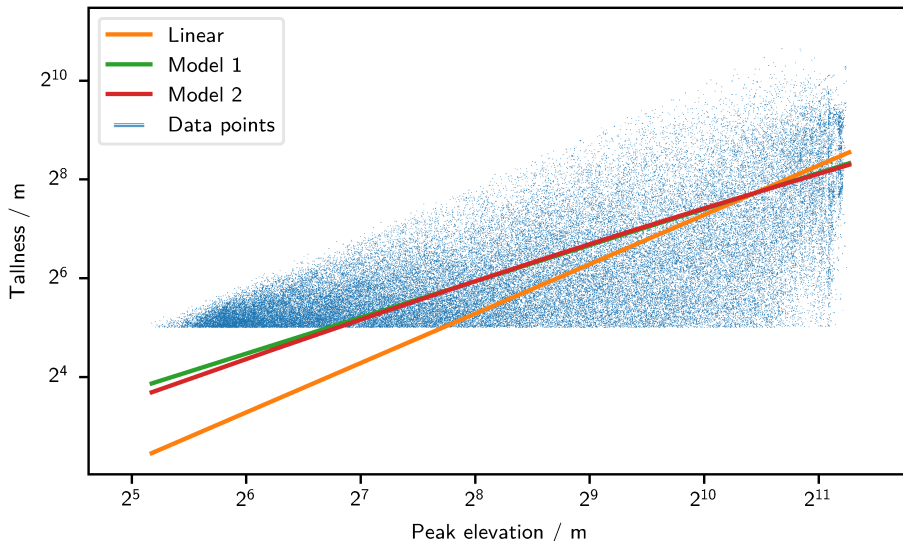


Figure 1.28.: Mountain tallness as a function of peak elevation in the southern parts of the Scandinavian mountains. The linear model uses eq. (1.8), with $A = 6.6$. “Model 1” uses eq. (1.7), with $z_0 = 0.93$ m, and $\alpha = 0.732$. “Model 2” uses eq. (1.6), with $A = 1000$ m, $z_0 = 5000$ m, $\alpha = 0.841$, and $\beta = 0.385$.

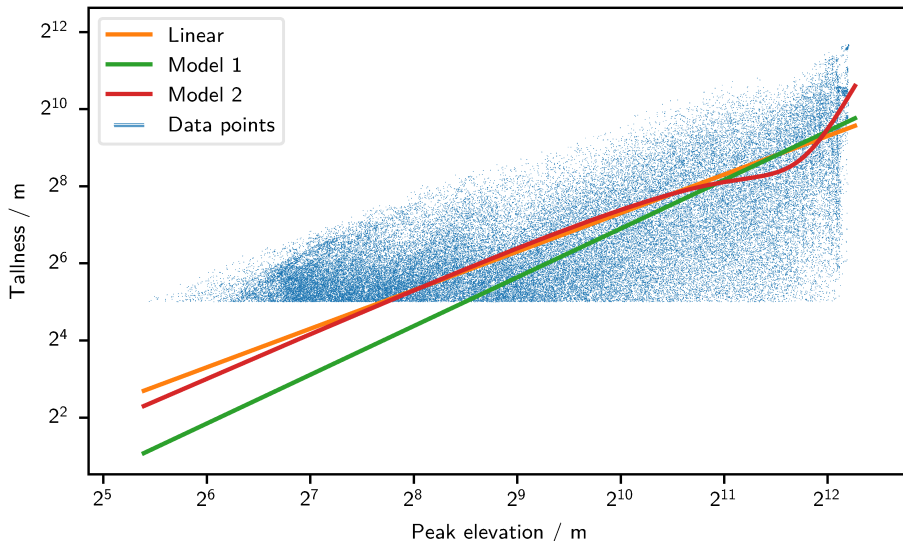


Figure 1.29.: Mountain tallness as a function of peak elevation in the Alps. The linear model uses eq. (1.8), with $A = 6.5$. “Model 1” uses eq. (1.7), with $z_0 = 23$ m, and $\alpha = 1.26$. “Model 2” uses eq. (1.6), with $A = 890$ m, $z_0 = 3500$ m, $\alpha = 1.17$, and $\beta = 3.74$.

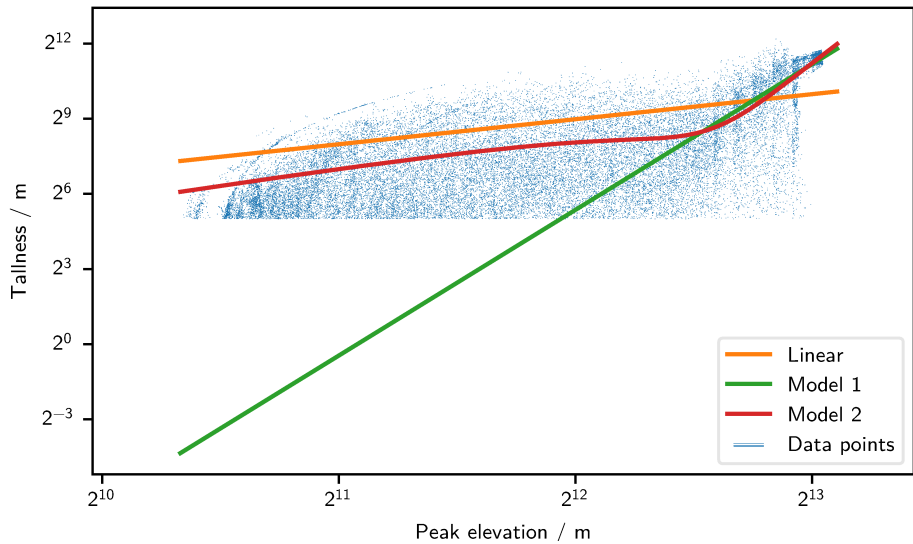


Figure 1.30.: Mountain tallness as a function of peak elevation in the Karakoram mountains. The linear model uses eq. (1.8), with $A = 8.1$. “Model 1” uses eq. (1.7), with $z_0 = 2200$ m, and $\alpha = 5.82$. “Model 2” uses eq. (1.6), with $A = 830$ m, $z_0 = 6200$ m, $\alpha = 1.54$, and $\beta = 6.11$.

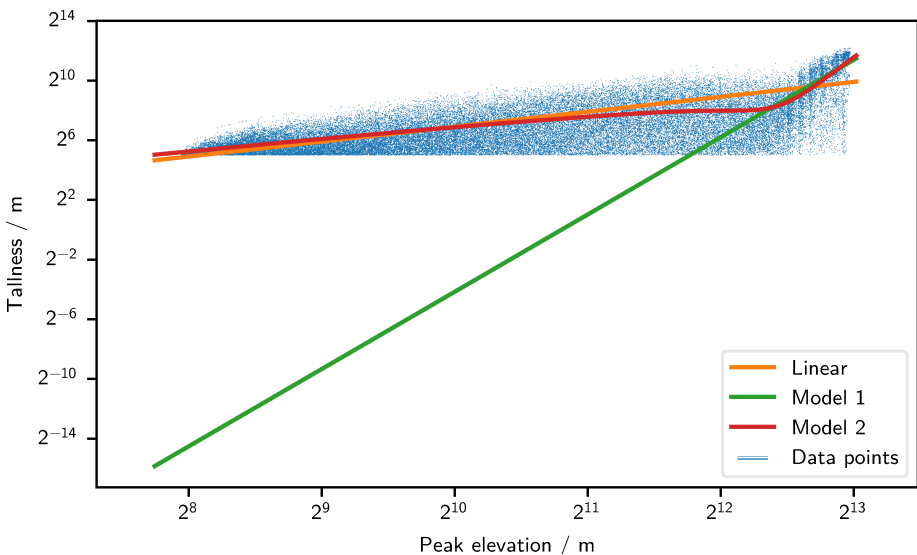


Figure 1.31.: Mountain tallness as a function of peak elevation in the western parts of the Himalayas. The linear model uses eq. (1.8), with $A = 8.5$. “Model 1” uses eq. (1.7), with $z_0 = 1800$ m, and $\alpha = 5.18$. “Model 2” uses eq. (1.6), with $A = 670$ m, $z_0 = 5600$ m, $\alpha = 0.910$, and $\beta = 5.67$.

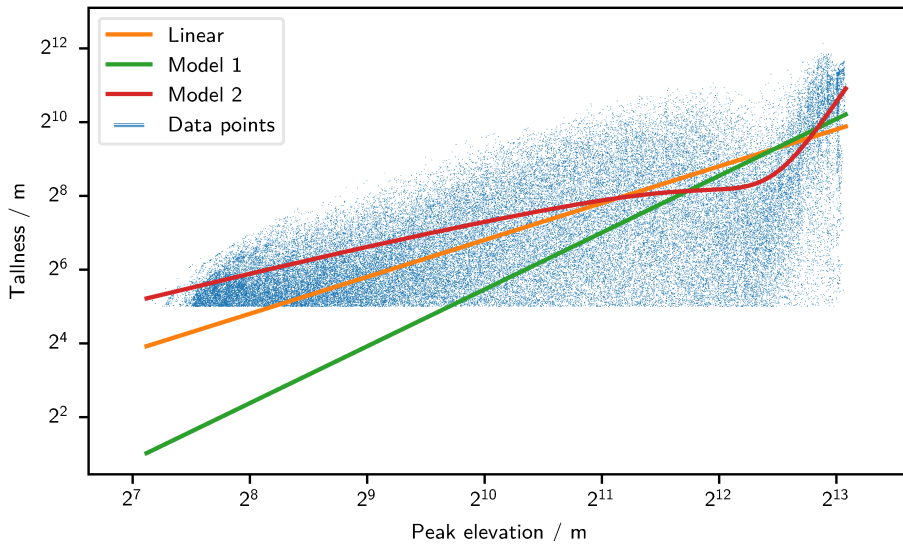


Figure 1.32.: Mountain tallness as a function of peak elevation in the central parts of the Himalayas. The linear model uses eq. (1.8), with $A = 9.1$. “Model 1” uses eq. (1.7), with $z_0 = 88$ m, and $\alpha = 1.54$. “Model 2” uses eq. (1.6), with $A = 790$ m, $z_0 = 5700$ m, $\alpha = 0.808$, and $\beta = 3.83$.

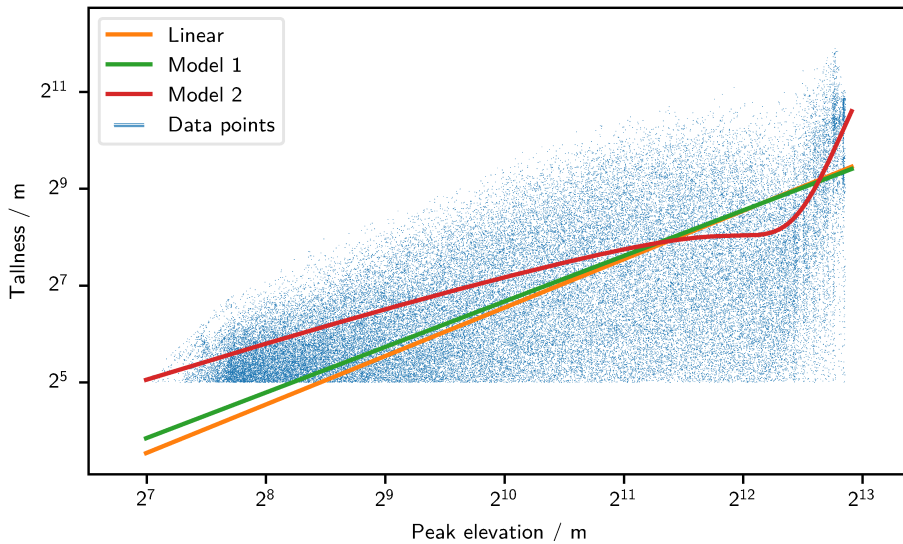


Figure 1.33.: Mountain tallness as a function of peak elevation in the eastern parts of the Himalayas. The linear model uses eq. (1.8), with $A = 11$. “Model 1” uses eq. (1.7), with $z_0 = 7.5$ m, and $\alpha = 0.940$. “Model 2” uses eq. (1.6), with $A = 700$ m, $z_0 = 5600$ m, $\alpha = 0.793$, and $\beta = 4.75$.

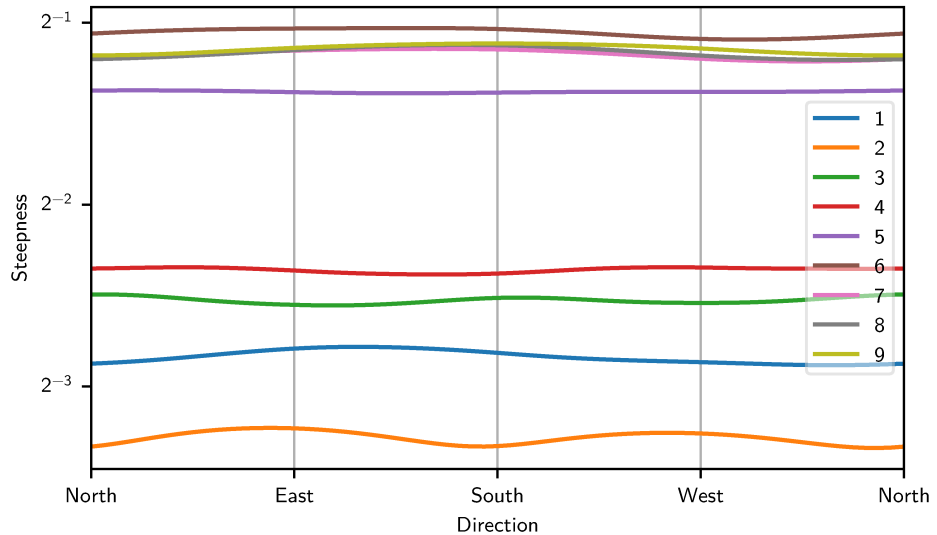


Figure 1.34.: The elevation distribution (measured in area per elevation) as a function of the elevation. Data-set numbering follows the order in table 1.2.

1.2.5. The average steepness as a function of direction

The directional dependency of the average steepness as defined by eq. (1.11) is shown in fig. 1.34. From this figure, it is clear that all data-sets show a directional dependency in steepness, though the variation in the Alps is relatively weak. Mountain ranges may show one or more steeper directions: The southern parts of the Ural mountains is a very “ideal” case where the north-south directionality gives rise to steeper slopes on the western and the eastern sides. Two scarp directions are also seen in the Scandinavian mountains, where the northern parts has a minimum from east south-east. The northern parts of the Ural mountains only feature one scarp direction (south-east), as is the case for the Himalayas and the Karakoram mountains, the latter having their scarp direction from the south.

The combination of the data presented in fig. 1.34 and fig. 1.13 is consistent with the results discussed section 1.2.3, with higher mountains being steeper, though fig. 1.34 shows that Karakoram, despite not featuring more than 4 of the 14 eight-thousanders, in average is steeper than any part of the Himalayas.

1.3. Mathematical models to create a height-map

Since the intent of the height-maps is only cover a small fraction of the earth surface, cartesian coordinates will be used. This eliminates the need for using scaling factors to compute derivatives, length elements, and area elements.

1.3.1. A simple noise-based model

A simple model for generating a height-map is to use normalized filtered noise as elevation function h_0 . If the filtered noise is denoted n_f

$$h_0 = \frac{n_f - \min_{(x,y) \in \Omega} n_f(x,y)}{\max_{(x,y) \in \Omega} n_f(x,y) - \min_{(x,y) \in \Omega} n_f(x,y)} \quad (1.12)$$

Now, let n denote an instance of uniformly distributed and white noise. The filtered noise n_f can then be produced by a convolution between n , and a suitable function G .

$$n_f = G * n \quad (1.13)$$

Assuming periodic boundary condition, it is possible to use fourier methods to efficiently implement eq. (1.13). Since n is uniformly distributed white noise, $\mathcal{F}n \sim n$. By using the convolution theorem,

$$n_f = G * n = \mathcal{F}^{-1}(\mathcal{F}(G * n)) = \mathcal{F}^{-1}(\mathcal{F}G \cdot \mathcal{F}n) = \mathcal{F}^{-1}(n \mathcal{F}G) \quad (1.14)$$

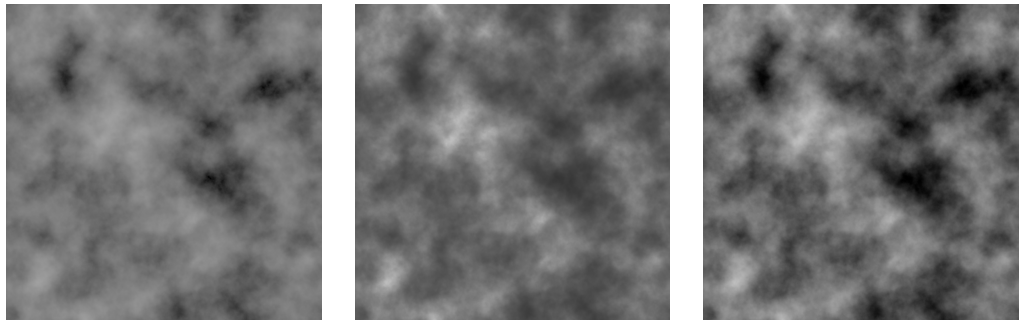
A possible choice for G is

$$G = \mathcal{F}^{-1} \left(\frac{1}{\sqrt{1 + \left(\frac{\xi^2}{\rho_x^2} + \frac{\eta^2}{\rho_y^2} \right)^2}} \right) \quad (1.15)$$

where ρ_x and ρ_y are scaling parameters that controls the size of the filter mask, and thus the “feature size”. Small values will result in larger feature sizes. If $\rho_x \neq \rho_y$, the filter will be anisotropic. Substituting eq. (1.15) into eq. (1.14) gives

$$n_f = \mathcal{F}^{-1} \left(\frac{n(\xi, \eta)}{\sqrt{1 + \left(\frac{\xi^2}{\rho_x^2} + \frac{\eta^2}{\rho_y^2} \right)^2}} \right) \quad (1.16)$$

The output of this model, with a certain value for ρ_x and ρ_y , is shown in fig. 1.35a and fig. 1.36a. The model works best for hillscapes. For mountainscapes, the shape of valleys differs from the shape of peaks, with valleys being smooth, and peaks being pointy. However, eq. (1.16) do not provide any statistical difference between peaks and valleys, and so does not h_0 , since eq. (1.12) is only affine. A way to



(a) Linear transfer function, $h = ah$ (b) Exponential transfer function, $h = 2^{b(h_0-1)}$ (c) Power transfer function, $h = h_0^c, c > 1$

Figure 1.35.: Filtered noise given by eq. (1.12) with n_f given by eq. (1.16). The values of h_0 has been transformed by applying different transfer function types: Linear, exponential, and power. The parameters a and b has been chosen such that the difference in root mean square to fig. 1.35c is minimized.

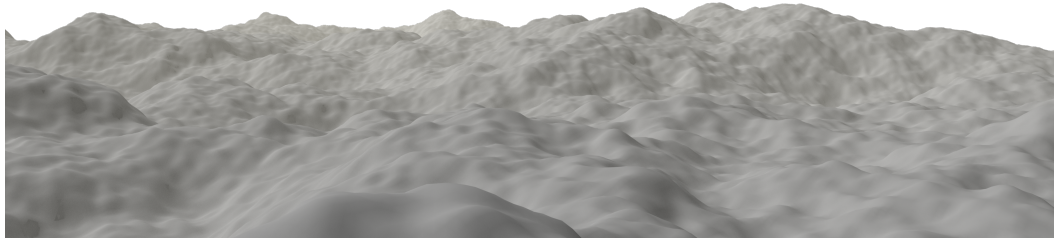
enhance the pointiness of peaks compared to valleys is to use a non-linear pixel-wise transformation h on h_0 . The requirement of h is that is defined on the range of n_f , which is $[0, 1]$. Moreover, its first and second derivatives on that interval should be positive. There are many options for h that fulfils these criteria, the most basic ones being $\exp(\kappa h_0)$, and h_0^κ , for some parameter κ . These corresponds to eq. (1.4) with $\alpha = 1$, and $\alpha \in]0, 1[$ respectively.

The fact that both the exponential transfer function (whose effect is shown in fig. 1.35b), and the the power transfer function (whose effect is shown in fig. 1.35c) has a positive second derivative means that they increase contrast between peaks and valleys. One difference is in what happens to locations with lower elevations. Since $\exp(x) > 0$, all locations will get an uplift. This makes the transition between valleys and mountain faces smooth. A power function does the opposite. Since

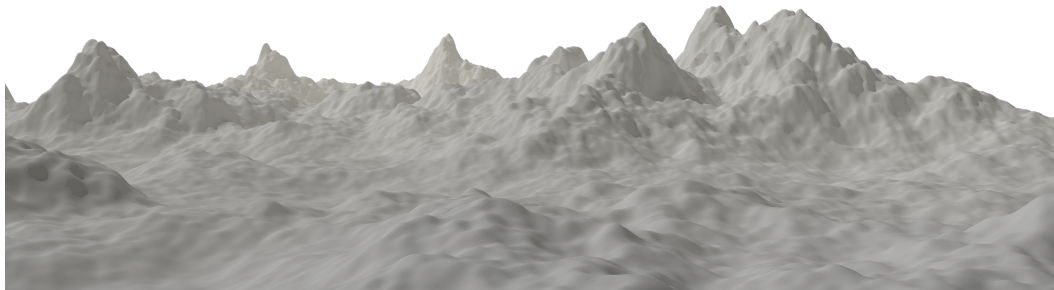
$$\begin{cases} x^c < x & , x < 1 \\ x^c > x & , x > 1 \end{cases}$$

lower values become lower, and higher values become higher. This means that the transition between mountain faces and valleys becomes more visible. The smoother nature of the exponential transfer function means that it can be suitable for more eroded mountains. However, from the results in section 1.2.3, a power law should work quite well for lower terrain as well.

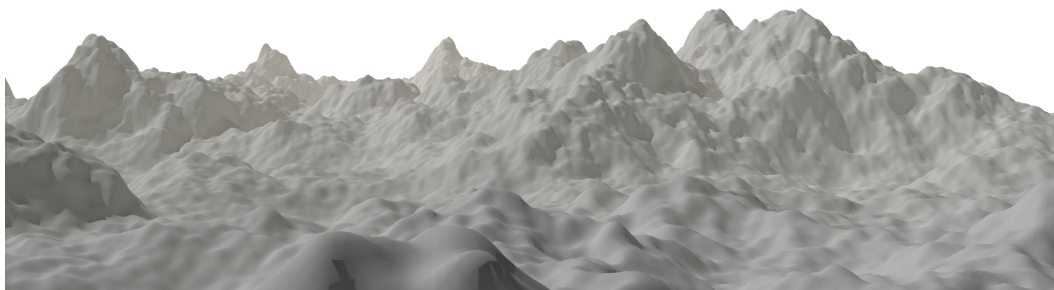
To get a better understanding of what the resulting terrain would look like, it may be useful to have renderings of landscapes created using the height-maps in fig. 1.35. Such renderings can be found in fig. 1.36. From fig. 1.36a it is clear that raw filtered noise gives smooth bumps of multiple sizes. Again, such data is useful to create hills, or to create local height variations. The non-linear transfer functions (figs. 1.36b and 1.36c) indeed increases the contrast between peaks and valleys. When comparing fig. 1.36b to fig. 1.36c, it is clear that the former keeps



(a) A rendering using fig. 1.35a



(b) A rendering using fig. 1.35b



(c) A rendering using fig. 1.35c

Figure 1.36.: Renderings of a landscape using the height-maps in fig. 1.35. All renderings have been shot from the same camera angle. The aspect ratio has been set to 2.4 : 1, and the horizontal field-of-view to 54.3°. For comparison with real data, see figs. 1.8 and 1.9.

ridges at a bit higher elevation. As a consequence, the exponential transfer function makes the highest peaks a lot steeper. This can be seen by looking at the third peak from the left.

Before concluding the discussion of the use to create filtered noise in height-map generation, it should be noted that there are many variants of this model. For example, it is possible to pass h through another filter, and blend the outputs with h to make smoother valleys. It is also possible to combine an exponential transfer function with the power transfer function to get a more sophisticated one, such as $h = \max(2^{b(h_0-1)}, h_0^c)$. The result of the latter, is shown in fig. 1.37.

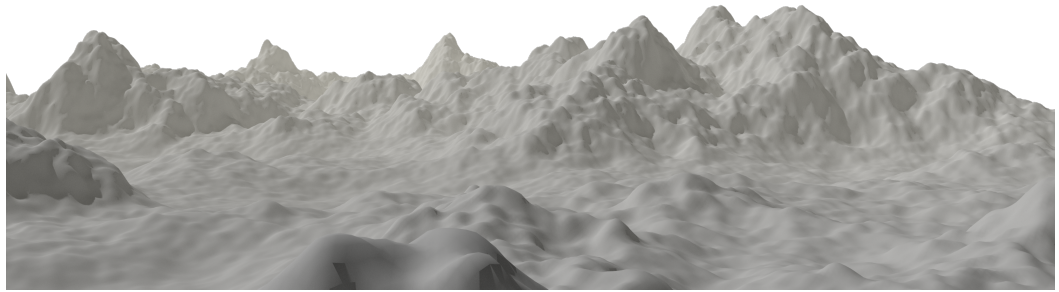


Figure 1.37.: A rendering of taking the max of figs. 1.35b and 1.35c. The aspect ratio has been set to 2.4 : 1, and the horizontal field-of-view to 54.3°. For comparison with real data, see figs. 1.8 and 1.9.

Bibliography

- [1] Torbjörn Rathsman (2022), geotiff-analyzer.
<https://github.com/milasudril/geotiff-analyzer/tree/e0bbc3fbed5f55e38474892a57d47b99edac5317>
- [2] Eric Jones and Travis Oliphant and Pearu Peterson and others (2001–). SciPy: Open source scientific tools for Python. <http://www.scipy.org>. Accessed: 2022-05-26
- [3] European Space Agency, Sinergise (2021). Copernicus Global Digital Elevation Model. Distributed by OpenTopography. <https://doi.org/10.5069/G9028PQB>. Accessed: 2022-05-21
- [4] Arne Persson, Lars-Christer Böiers (2008). Analys i flera variabler Upplaga 3:5. ISBN 978-91-44-03869-8

A. Scaling factors in geodetic coordinates

The GeoTIFF standard requires that the pixel coordinates are mapped using (translated) geodetic coordinates. The horizontal coordinate is mapped to the longitude λ and the vertical coordinate is mapped to the latitude ϕ . The pixel intensity is used to store the local elevation z . To convert geodetic coordinates into cartesian coordinates (X, Y, Z) , the transformation is

$$\begin{cases} X = (N + z) \cos \phi \cos \lambda \\ Y = (N + z) \cos \phi \sin \lambda \\ Z = \left(\frac{R_p^2}{R_e^2} N + z \right) \sin \phi = \left(\left(\frac{R_p}{R_e} \right)^2 N + z \right) \sin \phi \end{cases} \quad (\text{A.1})$$

where

$$N = \frac{R_e^2}{\sqrt{R_e^2 \cos^2 \phi + R_p^2 \sin^2 \phi}} = R_e \frac{1}{\sqrt{\cos^2 \phi + \left(\frac{R_p}{R_e} \sin \phi \right)^2}} \quad (\text{A.2})$$

[4], and R_p and R_e designates the polar and equatorial radius respectively.

From eq. (A.1), it is apparent that further expressions will be easier to work with under the substitution $r = \frac{R_p}{R_e}$. If $r = 1$, the transformation reduces to regular spherical coordinates. In reality, $R_p = 6357$ km and $R_e = 6378$ km. The difference between these values is comparable to the maximal expected elevation, which is around 8.8 km. Thus, the full model with $r \neq 1$ has to be used.

For an orthogonal coordinate system, such as geodetic coordinates, the scaling factor a_k , in the direction of u_k is

$$a_k = \left| \frac{\partial \mathbf{r}}{\partial u_k} \right| \quad (\text{A.3})$$

and

$$\frac{\partial f}{\partial x_k} = \frac{1}{a_k} \frac{\partial f}{\partial u_k}$$

Here, x_k is the k -th component of the cartesian coordinate system aligned with the tangent (hyper-)planes of the coordinate transformation functions, computed at the point of interest. There is also the distance function

$$|\mathrm{d}\mathbf{r}| = \sqrt{\sum_k a_k^2 (\mathrm{d}u_k)^2} \quad (\text{A.4})$$

, and the area elements

$$\{dA\}_k = \{a_l du_l \cdot a_m du_m\}_{l < m} \quad (\text{A.5})$$

In the case of eq. (A.1), $u_0 = \lambda$, $u_1 = \phi$, $u_2 = z$. Since height-maps are 2-dimensional, f is a function of ϕ and λ only. Also, vertical distances are not interesting for this study. Thus only a_ϕ and a_λ need to be computed. From eq. (A.3),

$$a_\lambda = \sqrt{\left(\frac{\partial X}{\partial \lambda}\right)^2 + \left(\frac{\partial Y}{\partial \lambda}\right)^2 + \left(\frac{\partial Z}{\partial \lambda}\right)^2} \quad (\text{A.6})$$

, and

$$a_\phi = \sqrt{\left(\frac{\partial X}{\partial \phi}\right)^2 + \left(\frac{\partial Y}{\partial \phi}\right)^2 + \left(\frac{\partial Z}{\partial \phi}\right)^2} \quad (\text{A.7})$$

All functions in eq. (A.1) can be written on the form $(cN + z)g(\phi, \lambda)$ where g is a suitable function. By the product rule,

$$\frac{\partial}{\partial \lambda} ((cN + z) \cdot) = c \frac{\partial N}{\partial \lambda} \cdot + (cN + z) \frac{\partial}{\partial \lambda} = (cN + z) \frac{\partial}{\partial \lambda} \quad (\text{A.8})$$

and

$$\frac{\partial}{\partial \phi} ((cN + z) \cdot) = c \frac{\partial N}{\partial \phi} \cdot + (cN + z) \frac{\partial}{\partial \phi} \quad (\text{A.9})$$

, with

$$\frac{\partial N}{\partial \phi} = R_e \frac{(1 - r^2) \cos(\phi) \sin(\phi)}{(\cos^2 \phi + r^2 \sin^2 \phi)^{\frac{3}{2}}}$$

From eq. (A.7), and eq. (A.6), 6 derivatives needs to be computed: $\begin{matrix} \frac{\partial X}{\partial \lambda} & \frac{\partial Y}{\partial \lambda} & \frac{\partial Z}{\partial \lambda} \\ \frac{\partial X}{\partial \phi} & \frac{\partial Y}{\partial \phi} & \frac{\partial Z}{\partial \phi} \end{matrix}$.

Using eqs. (A.8) and (A.9)

$$\frac{\partial X}{\partial \lambda} = -(N + z) \cos \phi \sin \lambda \quad (\text{A.10a})$$

$$\frac{\partial Y}{\partial \lambda} = (N + z) \cos \phi \cos \lambda \quad (\text{A.10b})$$

$$\frac{\partial Z}{\partial \lambda} = 0 \quad (\text{A.10c})$$

$$\frac{\partial X}{\partial \phi} = \frac{\partial N}{\partial \phi} \cos \phi \cos \lambda - (N + z) \sin \phi \cos \lambda \quad (\text{A.10d})$$

$$\frac{\partial Y}{\partial \phi} = \frac{\partial N}{\partial \phi} \cos \phi \cos \lambda - (N + z) \sin \phi \sin \lambda \quad (\text{A.10e})$$

$$\frac{\partial Z}{\partial \phi} = r^2 \frac{\partial N}{\partial \phi} \sin \phi + (r^2 N + z) \cos \phi \quad (\text{A.10f})$$

In case of $r = 1$, eq. (A.7), and eq. (A.6) reduces to the scaling factors for spherical coordinates, because $N = R_e$.